Marine Carbohydrates in Arctic Aerosol Particles and Fog – Diversity of Oceanic Sources and Atmospheric Transformations

Sebastian Zeppenfeld[1], Manuela van Pinxteren[1], Markus Hartmann[2], Moritz Zeising[3], Astrid Bracher[3,4], and Hartmut Herrmann[1]

1 Atmospheric Chemistry Department (ACD), Leibniz-Institute for Tropospheric Research (TROPOS), Leipzig, Germany
2 Atmospheric Microphysics (AMP), Leibniz-Institute for Tropospheric Research (TROPOS), Leipzig, Germany
3 Alfred-Wegener-Institute Helmholtz Centre for Polar and Marine Research, Bremerhaven, Germany
4 Institute of Environmental Physics, University of Bremen, Bremen, Germany

*Correspondence to*: Hartmut Herrmann (herrmann@tropos.de)

Abstract

Carbohydrates, produced and released by marine microorganisms in the ocean, enter the atmosphere as part of sea spray aerosol (SSA) and can influence fog and cloud microphysics by acting as cloud condensation nuclei (CCN) or ice nucleating particles (INP). Particularly in the remote Arctic region, significant knowledge gaps persist about the sources, the sea-to-air transfer mechanisms, atmospheric concentrations, and processing of this substantial organic group. In this study, Wwe present the results of a ship-based field study conducted from May to July 2017 in the Fram Strait, Barents Sea and central Arctic Ocean about the sea-air transfer of marine combined carbohydrates (CCHO) from concerted measurements of the bulk seawater, the sea surface microlayer (SML), aerosol particles and fog. In seawater, CCHO ranged between 22–1070 $\mu g\ L^{-1}$ with large differences among the different sea-ice-related sea surface compartments: ice-free ocean, marginal ice zone (MIZ), open leads/polynyas within the pack ice and melt ponds. Enrichment factors in the SML (EF_{SML}) relative to the bulk water were very variable in the dissolved ($EF_{SML,dCCHO}$: 0.4–16) and particulate ($EF_{SML,pCCHO}$: 0.4–49) phases with highest values in the MIZ and aged melt ponds. In the atmosphere, CCHO appeared in super- and submicron aerosol particles ($CCHO_{aer,super}$: 0.07–2.1 $ng\ m^{-3}$; $CCHO_{aer,sub}$: 0.26–4.4 $ng\ m^{-3}$) and fog water ($CCHO_{fog,liquid}$: 18–22000 $\mu g\ L^{-1}$; $CCHO_{fog,atmos}$: 3–4300 $ng\ m^{-3}$). The enrichment factors for the sea-air transfer were calculated for super- and submicron aerosol particles and fog, however strongly varied depending on which of the sea-ice-related sea surface compartments waswere assumed as the oceanic emission source. Finally,

Formatiert: Tiefgestellt

1

we observed a quick atmospheric aging of CCHO after their emission with indications for both biological/enzymatic processes (based on very selective changes within the monosaccharide compositions of CCHO) and abiotic degradation (based on the depolymerization of long-chained CCHO to short free monosaccharides). All in all, the present study highlights the diversity of marine emission sources in the Arctic Ocean and atmospheric processes influencing the chemical composition of aerosol particles and fog.
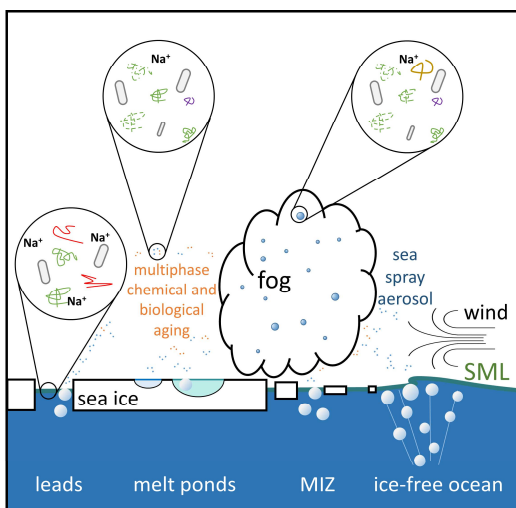
TOC Figure

1. Introduction

Sea spray aerosol (SSA) represents~~is~~ one of the major aerosol species in the lower troposphere over the remote Arctic Ocean, particularly during the ~~boreal~~ spring and summer months in the Northern Hemisphere (Chi et al., 2015; Hara et al., 2003; Kirpes et al., 2018; May et al., 2016). Depending on the size distribution and chemical composition, SSA particles strongly contributes~~s~~ to the populations of cloud condensation nuclei (CCN) and ice nucleating particles (INP) affecting the polar radiative budget through the formation of liquid droplets and ice crystals in fog and clouds (DeMott et al., 2016; Lawler et al., 2021; McCluskey et al., 2018; Penner et al., 2001; Schiffer et al., 2018; Wilbourn et al., 2020). Notably in the Arctic, one of the regions most affected by global warming, there is still a lack of knowledge about the relationship between the formation and evolution of clouds and specific chemical properties of ~~primary marine aerosol~~SSA particles (Wendisch et al., 2023).

SSA is emitted directly from the ocean surface through wind-driven processes and, as a consequence, contains the salts and the organic matter (OM) present in seawater, including carbohydrates (CHO) as one of the largest identified organic fractions (Quinn et al., 2015 and references therein). In microalgae, bacteria and also more complex marine organisms (e.g. kelp, krill), carbohydrates have important metabolic, structural and protective functions or are released in response to environmental stress, such as freezing or lack of nutrients (Krembs et al., 2002; Krembs and Deming, 2008; McCarthy et al., 1996; Mühlenbruch et al., 2018; Suzuki and Suzuki, 2013; Wietz et al., 2015). In seawater, most carbohydrates appear as linear or branched oligo- and polysaccharides, commonly referred to as combined carbohydrates (CCHO). They can be found in both dissolved (dCCHO) and particulate (pCCHO) phases, distinguished operationally by a 0.2 µm filtration.~~In seawater, the majority of carbohydrates appears as linear or branched oligo- and polysaccharides, commonly referred to as combined carbohydrates (CCHO), both in the dissolved (dCCHO) and the particulate (pCCHO) phases.~~ These macromolecules consist of several monosaccharides, such as hexoses, pentoses, deoxy sugars, amino sugars, uronic acids and amino sugar acids, which are connected via glycosidic bonds (Benner and Kaiser, 2003; Engel and Händel, 2011; Panagiotopoulos and Sempéré, 2005). Most CCHO are quite stable within the marine environment unless they are either hydrolyzed in the presence of specific enzymes or in a very acidic setting (Arnosti, 2000; Panagiotopoulos and Sempéré, 2005). Heterotrophic bacteria use extracellular enzymes to selectively degrade CCHO into absorbable shorter molecules leaving a certain part as recalcitrant, more persistent OM (Alderkamp et al., 2007; Becker et al., 2020; Goldberg et al., 2011; Wietz et al., 2015). While pCCHO is mostly attributed to recent productions by local phytoplankton indicated by high positive correlations with total chlorophyll a (TChl-a), dCCHO appears to be the result of more complex metabolic and transformation processes after its release (Becker et al., 2020; Fabiano et al., 1993; Goldberg et al., 2011; Zeppenfeld et al., 2021a). In contrast,

3

78   dissolved free carbohydrates (*d*FCHO), short sugars in their monomer form, are quickly consumed by

79   marine microorganisms resulting in much lower concentrations of *d*FCHO compared to CCHO in

80   ambient seawater (Engbrodt, 2001; Engel and Händel, 2011; Ittekkot et al., 1981; Zeppenfeld et al.,

81   2020).

82   In the remote marine atmosphere, carbohydrates are ~~assumed~~ suggested to significantly impact cloud

83   properties by contributing to both the CCN and INP populations (Alpert et al. 2022; Leck et al., 2013;

84   Orellana et al., 2011; van Pinxteren et al., 2022). Carbohydrates appear both in super- and submicron

85   SSA particles (Aller et al., 2017; Leck et al., 2013; Russell et al., 2010; Zeppenfeld et al., 2021a), most

86   likely resulting from their emission from the surface of the ocean after bubble bursting as part of jet

87   and film droplets (Veron, 2015; Wang et al., 2017). In addition to the bulk surface seawater, the sea

88   surface microlayer (SML) as the uppermost layer of the oceanic water column is an important source

89   of OM, and thus marine carbohydrates, in the SSA. The SML is described as a gelatinous film on top of

90   the ocean, which is often enriched in surface-active substances or buoyant gel particles compared to

91   the underlying bulk water (Engel et al., 2017; Wurl et al., 2009, 2011; Zäncker et al., 2017). Entrained

92   air bubbles rise within the upper part of the water column~~, scavenges~~ collecting surface-active

93   organics on the bubble surfaces from the ~~surface~~ bulk seawater ~~and pass the thin SML~~(Burrows et al.,

94   2014). Eventually they~~-~~ pass the thin SML and burst there releasing film and jet droplets containing a

95   mixture of substances found within the bulk water and the SML (Burrows et al., 2014). At the same

96   time, surfactants, exopolymers and microgels in the SML increase the stability of the cap films of the

97   bubbles, extend their lifetimes and enable the drainage of water-soluble compounds (Bigg and Leck,

98   2008; Bikerman, 2013; Sellegri et al., 2006). Consequently, the sea-air transfer occurs in a chemo-

99   selective manner leading to a strong size-dependent enrichment of surface-active organics relative to

100   water-soluble sodium (Na^+) and, hence, a relative chemical composition of SSA different to the surface

101   seawater (Facchini et al., 2008; O'Dowd et al., 2004; van Pinxteren et al., 2017; Prather et al., 2013;

102   Quinn et al., 2015; Triesch et al., 2021a, b). These chemo-selective enrichments of organic substances

103   in the SSA relative to bulk water, especially in the submicron size range, usually exceed the enrichments

104   in the SML by orders of magnitude (van Pinxteren et al., 2017; Schmitt-Kopplin et al., 2012). The

105   underlying mechanisms for the chemo-selective sea-air transfer of carbohydrates, including co-

106   adsorption, are complex and subject of several recent and ongoing laboratory tank and modelling

107   studies (Burrows et al., 2016; Hasenecz et al., 2020; Schill et al., 2018; Xu et al., 2023). After their

108   emission, fresh SSA particles, including the contained carbohydrates, undergo atmospheric aging due

109   to a not yet well-understood interplay of several atmospheric processes, such as atmospheric

110   acidification, abiotic radical chemistry and biological and enzymatic modifications (Angle et al., 2021;

111   Hasenecz et al., 2020; Malfatti et al., 2019; Trueblood et al., 2019; Zeppenfeld et al., 2021a), potentially

112   also altering their microphysical properties.

4

Besides SSA, high concentrations of marine carbohydrates in fog and low-level clouds in the marine environment are plausible due to the high hygroscopicity of SSA serving as good CCN (Xu et al., 2022) transferring OM from the particle into the liquid phase, the high water-solubility of carbohydrates, and cloud-borne microorganisms potentially forming carbohydrates in-situ (Matulová et al., 2014). Only a few studies conducted at field sites exposed to marine air masses measured certain subgroups of carbohydrates, such as primary saccharides (Dominutti et al., 2022) or transparent exopolymer particles (TEP) (Orellana et al., 2011; van Pinxteren et al., 2022) so far in fog/clouds. However, the sources of marine carbohydrates in marine ambient fog/clouds, including dFCHO$_{fog}$ and CCHO$_{fog}$, and their relationship to the bulk seawater, SML and aerosol particles still lack elucidation.

During the summer months, the chemical compounds of natural SSA and marine fog can be studied in the Arctic Ocean due to the low influence of long-range transported anthropogenic pollution (Bozem et al., 2019; Schmale et al., 2021). However, the presence and seasonal evolution of Arctic sea ice divides this pristine region into a complex ensemble of several sea-ice-related sea surface compartments. These encompass the open leads - sea ice fractures with variable widths ranging from several to hundreds of meters - and polynyas, which are larger, more persistent areas of open water within the pack ice. These encompass the open leads - sea ice fractures with variable widths of several meters - and polynyas within the pack ice. Furthermore, there is the ice-free ocean, the marginal ice zone (MIZ) defined via by a sea ice concentration threshold between 15 and 80% (Rolph et al., 2020), and melt ponds forming and developing during the melting season on top of the ice floes. These environments are characterized by different chemical, physical and biological characteristics potentially influencing the quantity and properties of the SSA emitted. Recent studies observed, for instance, that the number and efficiency of Arctic INP are strongly dominated by the type of sea-ice-related sea surface compartments that the air masses had passed before sampling (Creamean et al., 2022; Hartmann et al., 2021; Papakonstantinou-Presvelou et al., 2022; Porter et al., 2022). However, the individual conclusions still appear controversial and might be biased by seasonal and interannual variabilities. Consequently, more systematic studies in the Arctic, also with regard to the chemical properties of the aerosol particles, are required to achieve more conclusive results.

To increase the knowledge about marine carbohydrates as important constituents of SSA and potential CCN and INP, we present here the results of a comprehensive field study conducted onboard the German icebreaker RV *Polarstern* from May to July 2017. We performed concerted measurements of bulk seawater, SML, size-resolved aerosol particles and fog water at different locations dominated by different sea-ice-related sea surface compartments (ice-free, leads/polynyas, MIZ, melt ponds) in the Arctic Ocean. All marine and atmospheric compartments are discussed and compared on absolute CCHO concentrations, calculated CCHO/Na$^+$ ratios, the relative monosaccharide contribution to CCHO

147 and the occurrence of *d*FCHO. The complex nature of these primary emission mechanisms and

148 subsequent atmospheric aging of marine CCHO in the Arctic Ocean are discussed in relation to our

149 findings. Our Arctic results are collated with those from the Southern Ocean at the Antarctic peninsula

150 during the austral summer, as presented in Zeppenfeld et al. (2021a) following a similar experimental

151 design. While both polar locations are remote marine regions with comparable meteorological

152 conditions during the sampling periods, the presence of Arctic sea ice adds another dimension of

153 complexity to data interpretation. Eventually, we disclose the complexity of the primary emission

154 mechanisms and subsequent atmospheric aging of marine CCHO in the Arctic Ocean.

2. Experimental

2.1 Study area and field sampling

Field samples were gathered during the PS106 (PASCAL/SiPCA) campaign (Macke and Flores, 2018; Wendisch et al., 2018) conducted from May to July 2017 on board the German icebreaker RV *Polarstern* in the Fram Strait, Barents Sea and central Arctic Ocean, including a period operating from a driftingn ice stationfloe camp period (035–164 June 2017) on board the German icebreaker RV *Polarstern*.

Marine SML and corresponding bulk water samples were collected at from various locations as shown in **Figure SI 1** (Figure SI 1). These include from the ice-free ocean (four sampling events), open water areas within the pack ice (20 sampling events, without distinguishing betweenopen open leads and polynyas within the pack ice (20 sampling events), the MIZ (five sampling events), and young and aged melt ponds (six sampling events) and the MIZ (five sampling events). Using visual characteristics, melt ponds were categorized as young (small, bluish, clear) or aged (larger, darker blue to greenish, and turbid with particulates and microalgae). To minimize contamination from exhausts and wastewater, water samples were taken at distances greater than 100 m from the ship. Seawater was collected either using a rubber boat or directly from the ice edge. SML samples were obtained by immersing a glass plate (length: 50 cm, width: 20 cm, thickness: 0.5 cm, sampling area: 2000 cm^2) vertically into the surface water and slowly withdrawing it at a speed of approximately 15 cm s^{-1} (van Pinxteren et al., 2012; Zeppenfeld et al., 2021a). The adhered SML film was drawn off the glass plate surface into a prewashed wide-neck plastic bottle by a framed Teflon wiper. The average thickness of the SML collected during this field study was 76±10 μm, which was calculated based on the volume of the SML sample collected, the area of the immersed glass plate and the number of dips as described by Cunliffe and Wurl (2014). Despite air temperatures during PS106 (median: -0.5°C; minimum: -7.6°C) hovering around or slightly below the freezing point of seawater, the SML remained unfrozen on the glass plate during sampling. The corresponding bulk water was taken from a defined depth of 1 m into LDPE bottles attached to a telescopic rod, except inat the bottom closed melt ponds where it was scooped from the bottom at approximately 20–40 cm depth. Whenever melt pond sampling took place, snow samples were collected from the ice floe surface roughly 10 m away from the melt pond. Before each sampling, the sampling containers were first rinsed with a few milliliters of the corresponding aqueous sample which was disposed immediately after. On board, small aliquots of the water samples were analyzed immediately for salinity using a conductivity meter (pH/Cond 3320, WTW), colored dissolved organic matter (CDOM) and particulate absorption (PAB), with more details in section 2.6. For later chemical analyses (inorganic ions, pH, carbohydrates) 500–1000 mLl of 0.2 μm filtered water sample

188 (dissolved fraction), 0.2 µm polycarbonate filters (particulate fraction) and field blanks were stored at
189 -20°C.

190 The sampling of ambient aerosol particles was conducted at the starboard side of RV *Polarstern* at the
191 top of the observation deck at a height of approx. 25 m above sea level as already described in Kecorius
192 et al. (2019). Size-segregated aerosol particles were sampled in five size ranges (stage 1: 0.05–0.14 µm,
193 stage 2: 0.14–0.42 µm, stage 3: 0.42–1.2 µm, stage 4: 1.2–3.5 µm, stage 5: 3.5–10 µm aerodynamic
194 particle diameter with a 50% cut-off) on aluminum foils by using two synchronized low-pressure Berner
195 impactors (Hauke, Austria) with a flow rate of 75 L min^{-1} and a sampling time of three to six days. To
196 avoid the condensation of atmospheric water and subsequent microbial activities on the aluminum
197 foils, a 3 m long heated tubes between the isokinetic inlets and the impactors reduced the relative
198 humidity of the sampled air to 75-80%, when the ambient relative humidity was higher. During this
199 field study, the difference of the temperatures of the ambient air at the inlet and the sampled air after
200 the heating never exceeded 9 K. Consequently, losses of semi-volatile compounds or changes by heat-
201 induced chemical reactions are expected to be neglectable. Furthermore, the Berner impactors were
202 thermally insulated by a polystyrene shell. After sampling, the foils were stored in aluminum containers
203 at -20°C until analysis. In this study, the results from stages 1-3, 4-5 and 1-5 were summed up as
204 submicron (sub), supermicron (super) and PM$_{10}$, respectively. Details about the size-resolved aerosol
205 particle samples and corresponding meteorological information are given in (Table SI 1~~Table SI 1~~, in
206 total 15 complete sets of Berner foils).

207 Close to the aerosol sampling, fog was collected using the Caltech Active Strand Cloud Collector Version
208 2 (CASCC2) as described by Demoz et al. (1996). Bulk fog droplets were impacted on Teflon strands
209 with a diameter of 508 µm and collected into a prewashed Nalgene polyethylene bottle. The flow rate
210 was 5.3 m^3 min and the 50% lower cut-off was determined to be approximately 3.5 µm. Further
211 information about the 22 fog samples collected during the PS106 campaign including meteorological
212 information can be found in Table SI 2~~Table SI 2~~ and in Hartmann et al. (2021).

2.2 Total aerosol particle mass concentrations

214 Before and after sampling, the aluminum foils were equilibrated (three days, 20°C, 50% relative
215 humidity) and weighed using a precise microbalance (Mettler Toledo XP2U, weighing error: ±4.6 µg).
216 Total particle mass concentrations (mass$_{aer, stage y}$) were calculated for each Berner stage as the ratio
217 between the difference of the absolute foil masses after and before sampling and the sampled air
218 volume. Afterwards, aluminum foils were divided for further chemical analyses.

2.3 OC/EC in aerosol samples

220 Organic carbon (OC_{aer}) and elemental carbon on Berner aerosol foils were determined as described by
221 Müller et al. (2010) using a two-step thermographic method (C/S MAX, Seifert Laborgeräte, Germany)
222 with a nondispersive infrared sensor.

223

224 2.4 Carbohydrates in aerosol particles, fog, snow, seawater and melt ponds

225 Marine carbohydrates in the particulate ($pCCHO$, >0.2 µm) and dissolved ($dCCHO/dFCHO$, <0.2 µm)
226 phases, including truly dissolved molecules and small colloids, were quantified from seawater and melt
227 pond samples following the protocol presented by Zeppenfeld et al. (2020, 2021a) using high-
228 performance anion-exchange chromatography with pulsed amperometric detection (HPAEC-PAD)
229 equipped with a Dionex CarboPac PA20 analytical column (3 mm × 150 mm) and a Dionex CarboPac
230 PA20 guard column (3 mm × 30 mm). The monosaccharides fucose (Fuc), rhamnose (Rha), arabinose
231 (Ara), galactose (Gal), glucose (Glc), xylose (Xyl), mannose (Man), fructose (Fru), galactosamine (GalN),
232 glucosamine (GlcN), muramic acid (MurAc), galacturonic acid (GalAc), and glucuronic acid (GlcAc) were
233 identified by their retention times. $dFCHO$ represent the sum of identifiable monosaccharides before,
234 and $dCCHO$ and $pCCHO$ additionally released after an acid hydrolysis (0.8 M HCl, 100°C, 20 h). CCHO is
235 the sum of $dCCHO$ and $pCCHO$. CHO represents the sum of CCHO and $dFCHO$, and consequently
236 encompasses all carbohydrates measured within this study. **Figure 1** ~~Figure 1~~ gives an overview of the
237 here used carbohydrate-related abbreviations. Marine carbohydrates in fog water, snow and extracts
238 from size-resolved aerosol particles were measured with ($CCHO_{fog}$, $CCHO_{aer}$) or without ($dFCHO_{fog}$,
239 $dFCHO_{aer}$) prior acid hydrolysis.

240
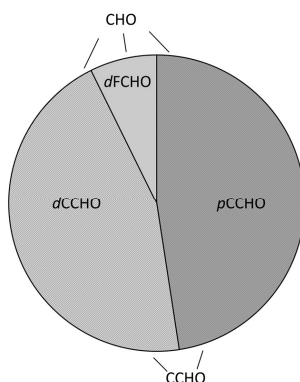
Figure 1. Overview of the abbreviations for carbohydrates (CHO) in seawater. CCHO: combined carbohydrates; $pCCHO$: particulate combined carbohydrates, $dCCHO$: dissolved combined carbohydrates; $dFCHO$: dissolved free carbohydrates.

247 2.5 Sodium and pH in aerosol particles, fog, seawater and melt ponds

Major inorganic ions, including sodium (Na^+), were determined from 0.45 µm filtered aqueous extracts of the size-resolved aerosol samples (50% of the Berner foil in 2 mL̶l̶ ultrapure water), fog water, diluted (1:15 000) seawater and melt pond samples using ion chromatography (ICS-3000, Dionex) as described by Müller et al. (2010). In this study, we discuss the results for Na^+ as a proxy for ~~primary sea spray~~SSA emissions in remote marine regions. Additionally, the pH was monitored by an additional autosampler sample conductivity and pH accessory (Dionex) in all seawater, melt pond and, whenever enough sample volume was available, in fog water.

2.6 Absorption by phytoplankton, non-algal particles and colored dissolved organic matter in seawater and melt pond samples

For the investigation of bio-optical parameters in seawater and melt pond samples, the particulate fraction was collected by filtering the water samples (5–500 mL̶l̶) onto glass-fiber filters (GF/F, Whatman), while the dissolved fraction was filtered through 0.2 µm Spartan syringe filters (Whatman, Germany) immediately after sampling. The GF/F filters were analyzed to determine the absorption spectra (i.e. 320–844 nm, 2 nm resolution) using the quantitative filtration technique with an integrative-cavity absorption meter setup (QFT-ICAM) as developed by Röttgers et al. (2016). We followed the protocol by Liu et al. (2018) for the instrument used here and the determination of the absorption coefficients by total particles (a_p440), phytoplankton ($a_{ph}440$) and non-algal particles ($a_{NAP}440$) at λ=440 nm.

The absorption for the dissolved fraction ($a_{CDOM}(λ)$) between 270 and 750 nm (1 nm resolution) were measured as triplicates using a long path length liquid waveguide capillary cell (LWCC) system following the procedure by Lefering et al. (2017) and including the correction for salinity effects by Röttgers et al. (2014) as described for our instrumentation in Álvarez et al. (2022). The absorption coefficients in the visible at 443 nm ($a_{CDOM}443$) and UV at 350 nm ($a_{CDOM}350$) bands were used as indicators of CDOM magnitude.

2.7 Supporting observations

The German research vessel *Polarstern* performs continuous meteorological surface measurements during times of ship operation. For this study, we used the data from the HMP155 thermometer/hygrometer probe (Vaisala), the ultrasonic anemometer (Thies Clima) and the FS11 visibility sensor (Vaisala) ~~each~~ installed at a height of 29 m, 39 m and 20 m above sea level, respectively. The quality-controlled data made available by the operators on the public repository PANGAEA (Schmithüsen, 2018, 2019) supported the interpretation of the results of this study.

The 120 h back-trajectories were computed for the sampling periods of the size-resolved aerosol particles and fog water events using the NOAA HYSPLIT model (Stein et al., 2015). The back-trajectories

281 were calculated on an hourly basis using the GDAS1 meteorological fields (Global Data Assimilation
282 System; 1° latitude/longitude; 3-hourly) and at arrival heights of 50, 250 and 1000 m. Sea ice
283 concentration data were retrieved from ERDDAP (Environmental Research Division's Data Access
284 Program), a data server maintained by NOAA (National Oceanic and Atmospheric Administration). The
285 MIZ was defined here as the oceanic region with a sea ice concentration between 15 and 80%. Data
286 on melt pond fractions were accessed from the sea ice remote sensing data achieve of the University
287 of Bremen (https://data.seaice.uni-bremen.de, Istomina (2020)).

288 2.8 Statistics, calculations and visualization

289 Statistical analyses, calculations and visualization were performed in OriginPro, Microsoft Excel and R
290 version 4.2.1 using the following packages: oce, ocedata, ncdf4, openair, ggplot2, reshape2, scales,
291 lubridate, cmocean, maps, mapdata, rgdal, raster, RColorBrewer, sp. Time-resolved back-trajectories
292 and sea ice maps were combined using R to compute and visualize the air mass history regarding the
293 sea-ice-related sea surface compartments that haves been passed. As a result, relative residence times
294 of the air masses over certain surface features (ice-free, MIZ, pack ice, land) 12 hours before sampling
295 were calculated based on defined thresholds for sea ice concentration: less than 15% for ice-free
296 ocean, 15-80% for MIZ and over 80% for pack ice. Based on the remote sensing data used, we did not
297 distinguish between open leads and melt ponds as the air traversed the pack ice. Box-whisker plots
298 represent the interquartile range (box), median (horizontal line within the box), average (open square)
299 and the minimum and maximum values of the datasets (whiskers). Measured mean values are given
300 together with the calculated standard deviations (±). Correlations between two measured variables
301 were expressed via the Pearson correlation coefficient R. The thresholds of significance were set for
302 the p-values 0.1, 0.05, 0.01 and 0.001.

<aside>Formatiert: Schriftfarbe: Automatisch</aside>

303 Enrichment factors for CCHO in the SML (EF$_{SML}$) relative to the corresponding bulk sample in different
304 sea-ice-related sea surface compartments (ice-free, leads/polynyas, MIZ, melt ponds) were calculated
305 based on **Formula 1** with $[x]_{SML}$ and $[x]_{bulk}$ representing the concentrations of either pCCHO or dCCHO.
306 For the calculation of enrichment factors of CCHO in aerosol particles on Berner stage y (EF$_{aer,stage\ y}$;
307 **Formula 2**) and fog water (EF$_{fog}$; **Formula 3**) relative to the bulk water samples, the ocean was assumed
308 as the most likely source of atmospheric Na$^+$. For the calculations of EF$_{aer}$ and EF$_{fog}$, we used the median
309 value of all CCHO$_{bulk}$ /and Na$^+_{bulk}$ ratios foundconcentrations of all individual bulk samp in the
310 samplesles attributed to a of a certain sea-ice-related sea surface compartment (ice-free,
311 leads/polynyas, MIZ, melt ponds) were averaged o over the whole campaign.

11

312

$$EF_{SML} = \frac{[x]_{SML}}{[x]_{bulk}} \qquad (1)$$

313

$$EF_{aer,stage\ y} = \frac{[x]_{aer,stage\ y}/[Na^+]_{aer,stage\ y}}{[x]_{bulk}/[Na^+]_{bulk}} \qquad (2)$$

314

315

$$(3)$$

$$EF_{fog} = \frac{[x]_{fog}/[Na^+]_{fog}}{[x]_{bulk}/[Na^+]_{bulk}}$$

316

317

3. Results and Discussion

The sources of ~~primary marine aerosol~~SSA particles, and hence <u>of</u> atmospheric marine carbohydrates<u>,</u> <u>microbial cells and fragments</u>, in the Arctic are diverse and influenced by the prevailing sea ice conditions. Here, we present the concentrations and relative compositions of CCHO in the SML and bulk water from the ice-free ocean, open leads and polynyas within the pack ice, melt ponds and the MIZ. After this, the different sea-ice-~~-~~related sea surface compartments are linked with the atmospheric CCHO found in ambient size-resolved aerosol particles and fog water. ~~T~~<u>Eventually, t</u>he ~~influence~~<u>influences</u> of the air mass history, enrichments of CCHO towards Na^+ during the sea-air transfer and secondary atmospheric transformations processes altering atmospheric CCHO are discussed.

3.1 Sea ice influences the properties of the sea surface water

Variable CCHO concentrations in the Arctic surface water. CCHO were found in the dissolved (dCCHO) and particulate (pCCHO) phases of the SML and bulk water samples collected from the ocean and the melt ponds during the PS106 campaign. Among all ~~these~~ aqueous samples<u>,</u> regardless of the sampling environment and depth (SML versus bulk), dCCHO (13–640 µg L^{-1}; $mean_{dCCHO}$ = 82±110 µg L^{-1}; n=70) and pCCHO (4–810 µg L^{-1}; $mean_{pCCHO}$ = 84±160 µg L^{-1}; n=70) <u>concentrations</u> were <u>highly</u>~~very~~ variable. <u>However, the minimum, maximum and mean values of both</u>~~The occurring minima, maxima and mean values of both,~~ dCCHO and pCCHO~~, however,~~ ranged within the same orders of magnitude. CCHO as the sum of dCCHO and pCCHO ranged between 22–1070 µg L^{-1} ($mean_{CCHO}$ = 166±250 µg L^{-1}; n=70).

Large differences in the mean values and standard deviations of CCHO were observed among the four sea-ice-~~-~~related sea surface compartments in the Arctic (leads/polynyas within the pack ice, MIZ, ice-free ocean, melt ponds) as shown in <u>**Figure 2**</u> ~~Figure 2~~a+b. The highest mean values for dCCHO and pCCHO were observed in the SML of the MIZ ($mean_{dCCHO, SML, MIZ}$ = 190±160 µg L^{-1}; $mean_{pCCHO, SML, MIZ}$ = 370±310 µg L^{-1}; n=5) and melt ponds ($mean_{dCCHO, SML, melt ponds}$ = 190±240 µg L^{-1}; $mean_{pCCHO, SML, melt ponds}$ = 200±310 µg L^{-1}; n=6), while the SML of the lead/polynya ($mean_{dCCHO, SML, lead/polynya}$ = 70±75 µg L^{-1}; $mean_{pCCHO, SML, lead/polynya}$ = 70±120 µg L^{-1}; n=20) and ice-free open ocean ($mean_{dCCHO, SML, ice-free}$ = 73±12 µg L^{-1}; $mean_{pCCHO, SML, ice-free}$ = 36±5 µg L^{-1}; n=4) samples tended to contain ~~much~~ less CCHO. The <u>lower SML</u> ~~lower~~ concentrations <u>from this study</u> ~~of the~~<u>for the</u> Arctic ice-free open ocean and ~~the~~ lead/polynya samples <u>align closely with several other investigations.</u> <u>Specifically, our results are comparable to Gao et al. (2012), who studied the SML of Arctic leads</u> <u>($mean_{dCCHO, SML, Arctic leads}$ = 163±104 µg L^{-1}; $mean_{pCCHO, SML, Arctic leads}$ = 35±25 µg L^{-1}; n=4), and Zeppenfeld et</u> <u>al. (2021), focusing on the</u> ~~were rather similar to the~~ ice-free part of the Southern Ocean west of the Antarctic peninsula <u>during the austral summer</u> ($mean_{dCCHO, SML, Southern Ocean}$ = 48±63 µg L^{-1};

13

351     $\text{mean}_{pCCHO,\,SML,\,Southern\,Ocean}$ = 72±53 µg L^{-1}; n=18~~; Zeppenfeld et al., 2021~~). Similarly, our data mirror

352   findings from ~~during the austral summer,~~ the tropical Cape Verde ($\text{mean}_{dCCHO,\,SML,\,Cape\,Verde}$ = 85±30 µg L^{-}

353   ^{1}; van Pinxteren et al., (2023)) and the Peruvian upwelling region ($\text{mean}_{dCCHO,\,SML,\,Peru}$ ≈ 92±32 µg L^{-1};

354   Zäncker et al., (2017)). Consequently, the Arctic MIZ and melt ponds, especially the aged ones with
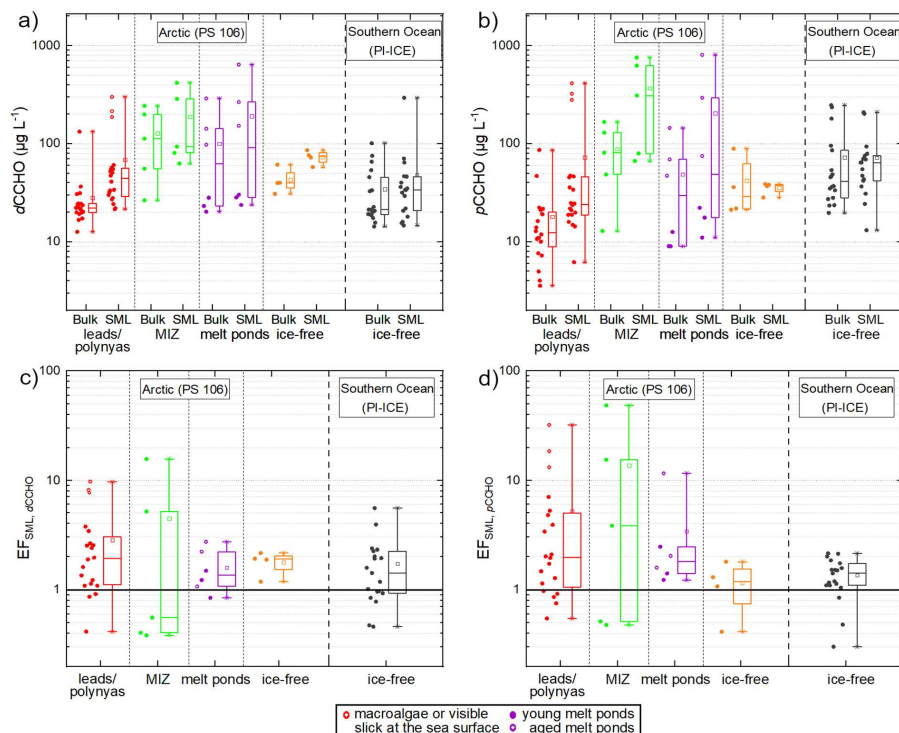
Figure 2. Scattered box-whisker plots showing the concentrations of a) *d*CCHO and b) *p*CCHO in the bulk and SML samples from the open leads and polynyas in the pack ice (red), the MIZ (green), ice-free open ocean (orange) and young and aged melt ponds (purple) collected during the PS106 campaign in the Arctic in comparison to the ice-free part of the Southern Ocean west of the Antarctic Peninsula investigated during the PI-ICE campaign in 2019 (black) as published in Zeppenfeld et al. (2021). EFs between SML and bulk water are shown in c) for *d*CCHO and d) for *p*CCHO. The black horizontal line represents an EF=1 meaning no enrichment or depletion.

355   advanced microbiological activities, stood out with elevated CCHO within the Arctic and also compared

356   to tropical and other polar regions.

357   ***Variable enrichments of CCHO in the SML.*** The enrichment factors (EF$_{SML}$) of the CCHO in the SML

358   relative to the corresponding bulk water ranged between 0.4 and 16 for *d*CCHO (**Figure 2**~~Figure 2~~c),

359   while the EF$_{SML}$ for *p*CCHO varied between 0.4 and 49 (**Figure 2**~~Figure 2~~d). ~~The vast majority, namely~~

360   ~~80%~~ of the SML samples were ~~, was~~ moderately ~~until~~ or highly enriched in marine carbohydrates with

361   only a few cases of depletion~~exceptions where they were depleted~~ (7 for *d*CCHO and 8 for *p*CCHO out

362   of 35 in total). With a median EF$_{SML,pCCHO,MIZ}$ value of 3.8 and a mean of 13.8, the enrichment of *p*CCHO

14

363 in the MIZ stood out compared~~in contrast~~ to the pCCHO in~~of~~ other sea-ice-related sea surface

364 compartments and to dCCHO ~~in general~~overall. However, it should be noted that the number of MIZ

365 samples was low and median and mean values were dominated by three sample pairs with very high

366 EF_{SML} values. Low to moderate enrichments for dCCHO and pCCHO were typically found in the

367 lead/polynya samples from the pack ice (median $EF_{SML,dCCHO,leads/polynyas}$=1.9; median

368 $EF_{SML,pCCHO,leads/polynyas}$=2.0, n=20). However, three lead samples showed quite high dCCHO & pCCHO

369 concentrations in the SML compared to the corresponding bulk samples resulting in high

370 $EF_{SML,dCCHO,leads/polynyas}$ up to 10 and $EF_{SML,pCCHO,leads/polynyas}$ up to 32. The exceptionally high EFs of these

371 three samples can be explained by the observation of slicks - visible films on the sea surface with

372 altered reflectance and typically high enrichments of organics (Cunliffe et al., 2013; Stolle et al., 2010;

373 Williams et al., 1986; Wurl et al., 2009) as well as the presence of macroalgae floating at the ocean's

374 surface near the sampling site. Even though the macroalgae were not collected themselves, their

375 exudates or fragments might have been released, accumulated and distributed in the SML close-by

376 and thus sampled. Consequently, the few samples with high EFs in open leads might rather represent

377 exceptional events as spatially small-scale phenomena.

378 The slight to high enrichments for dCCHO and pCCHO in this study are in good agreement with the

379 values reported by Gao et al. (2012), who determined $EF_{SML, dCCHO}$ between 3.5 and 12, and $EF_{SML, pCCHO}$

380 between 1.7 and 7.0 for open leads within the central Arctic Ocean. Furthermore, the $EF_{SML, dCCHO}$ of the

381 four Arctic sea-ice-related sea surface compartments reported here were not significantly different

382 compared to values found in the ice-free part of the Southern Ocean (ANOVA, one-way, 0.05

383 significance level). For the pCCHO, however, the average EF_{SML} in the Arctic MIZ was significantly higher

384 than the one of the Southern Ocean, whereas the $EF_{SML, pCCHO}$ of the ice-free ocean in the Arctic were

385 similar to the Southern Ocean.

386 For explaining the accumulation in the SML, previous studies proposed several mechanisms and

387 processes, which fundamentally differ for the dissolved and particulate carbohydrates. The enrichment

388 of pCCHO in the SML might be dominated by an interplay of density-related and wind-driven processes.

389 For instance, the positive buoyancy of TEP, a subgroup of pCCHO, leads to an upward flux serving as a

390 continual vehicle for marine organisms and attached chemical compounds (Azetsu-Scott and Passow,

391 2004; Mari et al., 2017). Furthermore, strong winds can cause a short-term mixing of the upper water

392 column reducing the EF_{SML} of particulates (Obernosterer et al., 2008) or TEP (Wurl et al., 2009; Zäncker

393 et al., 2021), while the wind-induced entrainment of air and the bubbling of seawater convert dissolved

394 negatively charged dCCHO and colloids into larger aggregates due to their sticky properties leading to

395 an enrichment of pCCHO in the SML (Passow, 2002; Robinson et al., 2019; Wurl et al., 2011). The

396 enrichment of dCCHO and also dFCHO in the SML is attributed to co-adsorption to other surface-active

15

compounds from the seawater matrix being scavenged at the surface of rising bubbles (Burrows et al., 2016; Hasenecz et al., 2020; Schill et al., 2018; Xu et al., 2023). Additionally, microbial processes in the SML could enhance the enrichment ~~through~~by in-situ ~~formation and release of~~ dCCHO production by micro- or macroalgae, while photolysis and enzymatic degradation of dCCHO into dFCHO by heterotrophic bacteria ~~would lead to a reduction~~could decrease the SML enrichment ~~of the enrichment in the SML~~. Specific to the Arctic, the release of meltwater from the sea ice could be an additional source for carbohydrates in the SML, considering the production of CCHO, exopolymeric substances (EPS) and TEP by sea ice algae and bacteria as a protection strategy against freezing damage and fluctuating salinity in sea ice (Aslam et al., 2016; Krembs et al., 2002; Krembs and Deming, 2008). This aligns well with the finding by Galgani et al. (2016) who observed labile, fresh OM in the SML of melt ponds compared to the rather old, refractory nature of the SML in the surrounding open leads. ~~Aslam et al., 2016; Galgani et al., 2016; Krembs et al., 2002; Krembs and Deming, 2008).~~ Hence, melting~~This~~ of sea ice could explain the extraordinarily high EF$_{SML}$ observed in some, but not all, SML samples from the MIZ and melt ponds. In summary, several processes might be responsible for enrichment processes in the SML, especially in the Arctic, where the melting of sea ice could strongly bias the physiochemical processes usually observed in controlled tank experiments.

High and low salinities due to freezing and melting of sea ice. While the surface seawater of the Arctic Ocean is very saline, the Arctic sea ice is much fresher due the separation into salt-free ice crystals and a salty brine during its formation from seawater and a subsequent salt loss from gravity drainage in winter and flushing during summer (Notz and Worster, 2009). During the late spring and summer period of this study, when strong melting of sea ice occurs, a large amount of freshwater enters the surface of the ocean creating inhomogeneities of salinity within the surface of the ocean. In both the ice-free ocean and the pack ice, where sea ice exists, but the melting rate is low, salinities of the SML and the bulk water ranged in this study between 30.9 and 34.5 (Zeppenfeld et al., 2019b), which is typical for the SML and the surface bulk water of the Arctic Ocean (Vaqué et al., 2021). Within the MIZ, where freshwater from melting sea ice quickly mixes with the salty ocean water, salinities were similar with values in this study between 30.1 and 33.4, however, also with an exception in the SML of 25.7. Melt ponds that were not yet joined at the bottom with the ocean below, were much fresher with lower and more variable salinities ranging from 4.3 to 19.5 (Zeppenfeld et al., 2019b). With a few exceptions, salinity discrepancies between the SML and the corresponding bulk water were small in most cases.

Sea-air transfer studies usually refer to open ocean scenarios with high salinities in the seawater and without the presence of melting sea ice. For the calculation of enrichment factors of organics in aerosol particles (EF$_{aer}$) or fog (EF$_{fog}$), the concentrations of Na$^+$ – a major compound of sea salt – in the

431 seawater bulk is included by default (see equations 2 and 3). However, the Arctic is a more complex
432 marine environment where salinities, and hence Na^+ concentrations, can vary widely as melting
433 progresses. This may strongly influence the mechanisms behind the bubble bursting process, the
434 $CCHO/Na^+$ ratios in the bulk seawater and the SML, and thus also the EF_{aer} and EF_{fog} as it will be
435 discussed in section 3.4. Consequently, the variability of salinity in Arctic seawater and melt ponds
436 should be considered for sea-air transfer studies that rely on Na^+ values.

437 ***Four sea-ice--related sea surface compartments with different characteristics.*** ~~In a nutshell, the~~The
438 high Arctic differs from other oceanic regions in the presence, formation and melting of sea ice creating
439 sea-ice--related sea surface compartments (ice-free, leads/polynyas, MIZ, melt ponds) with individual
440 biological and chemical characteristics, such as CCHO concentrations, enrichments in the SML and
441 salinities. This might potentially impact the transfer of substances from the ocean to the atmosphere,
442 chemo-selective enrichment processes of marine CCHO in the primary marine aerosol particles and
443 thus their microphysical properties. The next ~~chapters~~ sections will elucidate if and how these
444 differences within the individual compartments relate to $CCHO_{aer}$ and $CCHO_{fog}$.

3.2 Sea spray aerosol and therein contained combined carbohydrates

Breaking waves as the main mechanism for SSA emissions is not unambiguous in the Arctic. In the open ocean, the emission flux of SSA and hence its inorganic and organic constituents mainly ~~depends~~depend on the wind speed as the driving force for breaking waves and bubble bursting, and furthermore on the seawater temperature, salinity, wave properties and organic surface-active substances (Grythe et al., 2014). In this study, atmospheric sodium ($Na^+_{aer,PM10}$), the best tracer for SSA (Barthel et al., 2019), ranged between 12 and 765 ng m^{-3} (**Table SI 1**~~Table SI 1~~). $Na^+_{aer,PM10}$ showed a good correlation (R=0.80, p<0.001, **Figure 3a** ~~Figure SI 2a~~) with wind speed, measured at the sampling site and averaged over the sampling time, if all aerosol samples are included. However, the strength of this correlation decreased sharply (R=0.59, p<0.1), when only samples collected over the MIZ and the pack ice were included, while the few samples from the open ocean characterized by high Na^+ values were excluded. This is due to the presence of sea ice in the high Arctic, which likely alters and conceals the classical wind-driven mechanisms of breaking waves and bubble bursting resulting in SSA emission. Firstly, sea ice covers a significant part of the Arctic Ocean strongly reducing the area releasing SSA. Secondly, the presence of sea ice causes an attenuation of the high-frequency wind-sea waves, while longer waves, such as swells, can remain (Thomson, 2022). Consequently, the effect of wind on the SSA emission mechanisms within the open leads and the MIZ might be different than in the ice-free ocean. For those sea-ice-dominated compartments, alternative wind-independent sources of ascending bubbles were suggested, such as melting sea ice nearby, respiration of phytoplankton or sea-air heat exchange below the sea surface (Chen et al., 2022 and references therein). Thirdly, in contrast to other marine regions with quite homogeneous ocean salinities, and hence sodium concentrations, the salinities among the different Arctic sea-ice-related sea surface compartments are more variable due to the melting of sea ice. Previously, the results of a sea-air transfer tank experiment with artificial seawater showed the influence of salinity on the relative particle number concentrations of emitted SSA for salinities below 15 – values especially relevant for melt ponds in the Arctic – while changes at higher salinities did not result in a measurable effect (Zábori et al., 2012). Additionally, organics with potential surface-active properties are very variable in these disparate Arctic environments, as discussed for CCHO in ~~chapter~~ section 3.1. Organic surfactants can alter the ocean surface's ability to form whitecaps and the lifetime of bubbles (Bigg and Leck, 2008; Callaghan et al., 2012; Grythe et al., 2014) and therefore SSA properties.

Finally, blowing snow over the sea ice could serve as an additional~~, non-oceanic~~ source of atmospheric Na^+_{aer} when a certain air-temperature-dependent wind speed threshold is exceeded. (Chen et al., 2022; Gong et al., 2023; Huang and Jaeglé, 2017; Yang et al., 2008). Consequently, connections and correlations for the release of SSA particles in the heterogeneous high Arctic are more difficult to

479 explore than other marine environments without sea ice. It can be assumed that this complex setting

480 influences not only~~does not only influence~~ the release of ~~the~~ inorganic constituents from seawater,

481 but also its organic compounds, such as CCHO~~, too~~.
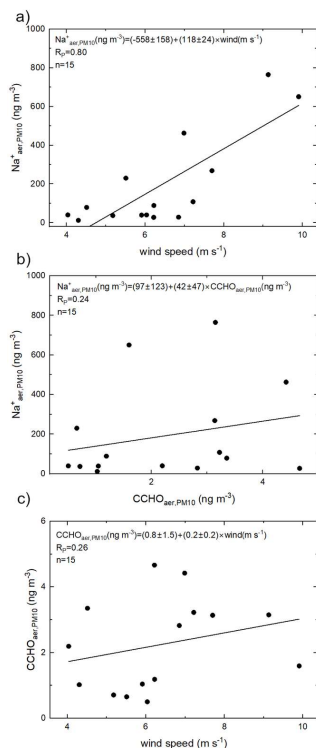
498 ***CCHO$_{aer}$ distributed in all size modes.*** During the PS106 campaign, the overall atmospheric

499 concentrations of $CCHO_{aer,PM10}$ ranged between 0.5 and 4.7 ng m^{-3} (**Table SI 1**~~Table SI 1~~). Combined

500 carbohydrates were found on both supermicron ($CCHO_{aer,super}$=0.07–2.1 ng m^{-3}) and submicron

501 particles ($CCHO_{aer,sub}$=0.26–4.4 ng m^{-3}). Thus, these $CCHO_{aer}$ values ranged within the same orders of

502 magnitude as in the Arctic studies by Karl et al. (2019) and Leck et al. (2013) or the study conducted at

503 the western Antarctic peninsula by Zeppenfeld et al. (2021a). $CCHO_{aer}$ appeared in all of the five size

504 classes in variable concentrations (**Figure 4**~~Figure 3~~a). Although the average concentrations were

505 similar on all stages, local maxima were observed on stages 2 (0.14–0.42 µm) and 5 (1.2–10 µm). A

506 similar size distribution of marine $CCHO_{aer}$ in these specific size ranges, but more pronounced, has been

19

507 already observed in the ice-free part of the Southern Ocean by Zeppenfeld et al. (2021a) explaining
508 these findings with a likely release of marine polysaccharides from the ocean as part of film and jet
509 droplets. Possibly, the aerosol size distribution of marine polysaccharides resulting from wind-driven
510 bubble bursting emissions are not as obvious in this Arctic study as it was in the ice-free Southern
511 Ocean due to the presence of Arctic sea ice suppressing and altering the local SSA emission
512 mechanisms as indicated in the previous section. The relative contribution of $CCHO_{aer}$ to $mass_{aer}$ varied
513 between 0.01% and 4% (**Figure 4**Figure 3b), while the carbon contained within the combined
514 carbohydrates (C-$CCHO_{aer}$) contributed 0.06 to 4.9% to the OC_{aer} in the size-resolved aerosol particles
515 (**Figure 4**Figure 3c). These contributions agree well with the findings in marine aerosol particles from
516 the Southern Ocean (Zeppenfeld et al., 2021a).

517
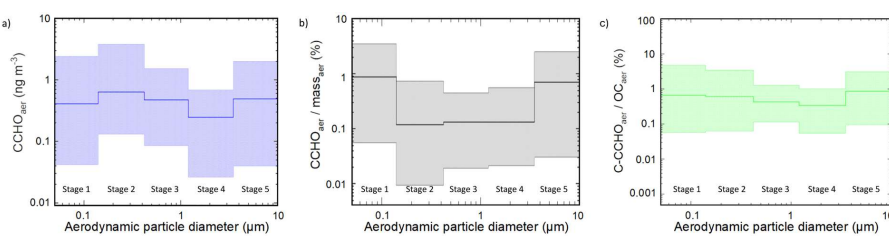
Figure 43. a) Concentration of combined carbohydrates in size-resolved aerosol particles ($CCHO_{aer}$), b) ratio of $CCHO_{aer}$ to the total particle mass concentration ($mass_{aer}$), c) ratios of carbon contained within the combined carbohydrates in aerosol particles (C-$CCHO_{aer}$) to organic carbon in aerosol particles (OC_{aer}). The bold lines represent the average concentrations during the PS106 campaign. The hatched areas show the range between the maximum and minimum values. The aerodynamic particle diameter refers to sampling conditions at relative humidity of max. 80%.

518 Unlike the study conducted in the Southern Ocean (Zeppenfeld et al., 2021a), $CCHO_{aer,PM10}$ in this study
519 showed no significant correlations with $Na^+_{aer,PM10}$ (R=0.24, p>0.1, **Figure 3b** Figure SI 2b) or wind speed
520 (R=0.26, p>0.1, **Figure 3c** Figure SI 2c). The presence of sea ice resulting in melt ponds and MIZ regions,
521 and the interplay of multiple emission mechanisms in the Arctic, as discussed earlier, could account
522 for this complexity. , which could be due to the complex marine environment and the relevance of
523 several emission mechanisms in the Arctic as discussed above. However, if the correlations are
524 resolved for the different Berner impactor stages (i.e. size ranges), a large variability can be observed
525 (**Figure 5** Figure 4). A higher correlation was found especially on stage 4 (1.2–3.5 µm) between
526 $CCHO_{aer,stage\ 4}$ and $Na^+_{aer,stage\ 4}$ (R=0.76, p<0.01), while the Pearson correlations coefficients for the other
527 Berner stages were much lower. This could indicate the same marine source and wind-driven emission
528 mechanism for both chemical constituents in this supermicron aerosol size mode, while other aerosol
529 size modes might have been influenced by atmospheric aging and wind-independent emission
530 mechanisms as already mentioned for Na^+_{aer} in the previous section. This observation agrees well with
531 the findings by Bigg and Leck (2008) and Leck (2002) reporting submicron polymer gel particles, likely

532 consisting of polysaccharides, in the atmosphere of the high Arctic containing almost no sea salt and

533 showing large similarities to those particles found in open leads close-by. This is quite surprising

534 considering that the mechanism of wind-driven wave breaking is quite limited due to the lack of long

535 fetches of open water (Held et al., 2011; Norris et al., 2011).

536
537
538
539
540
541
542
543

Figure 54. Pearson correlation coefficient R between $CCHO_{aer,stage\ y}$ and $Na^+_{aer,stage\ y}$ (solid line), between $CCHO_{aer,stage\ y}$ and the average wind speed (dashed line), and between $Na^+_{aer,stage\ y}$ and the average wind speed (dotted line) for each stage y of the Berner impactor.
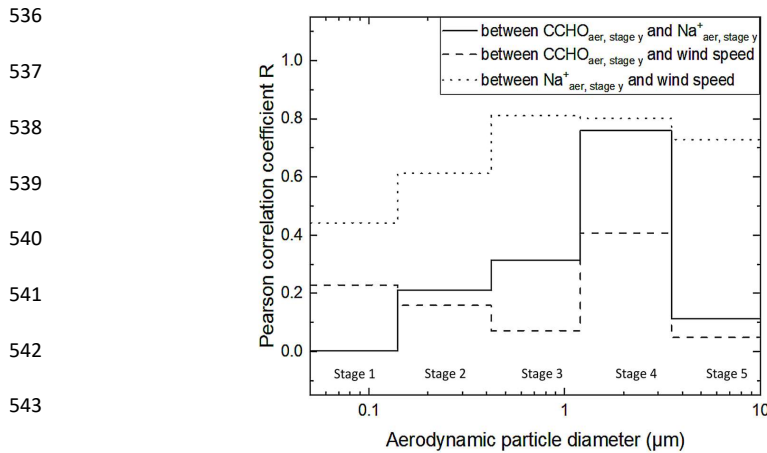
544 Blowing snow has been discussed as a possible additional source for atmospheric Na^+, raising the

545 question, if it could be a source for atmospheric carbohydrates, too. During this study, the

546 measurements of dFCHO and CCHO in five Arctic snow samples collected resulting in low values mostly

547 below the limits of detection. This finding supports the conclusion that blowing snow does not serve

548 as a competitive source for the emission of atmospheric marine carbohydrates.

21

3.3 Marine combined carbohydrates in fog

The concentrations of $Na^+_{fog, liquid}$ (1.7–903 mg L^{-1}; mean = 130±220 mg L^{-1}; n=22) and $CCHO_{fog, liquid}$ (18–22000 µg L^{-1}; mean = 1380±4600 µg L^{-1}; n=22) were very variable in fog water (**Table SI 2**~~Table SI 2~~). Atmospheric ~~fog~~ concentrations of these chemical constituents in fog droplets (indicated by the index 'fog,atmos') can be calculated under consideration of the liquid water content (LWC) during the fog events. Since LWC was not measured during PS106 directly, the LWC was approximated from the measured CCN concentrations at the lowest quality assured supersaturation of 0.15% and an assumed average droplet diameter of 17 µm. This approach result~~ing~~ed in ~~a~~ LWCs of 0.62 ±0.39 g m^{-3} for the fog collected over the North Sea and Norwegian Sea, and 0.12~~0~~±0.09~~27~~ g m^{-3} for the fog over the Arctic Ocean (Hartmann et al., 2021). Following this approach, atmospheric concentrations in fog ranged between 0.12 and 150 µg m^{-3} (mean = 25±43 µg m^{-3}; n=16) for $Na^+_{fog, atmos}$~~,~~ and between 3 and 4300 ng m^{-3} (mean = 390±1100 ng m^{-3}; n=16) for $CCHO_{fog, atmos}$, respectively. These atmospheric concentrations in fog are for both $Na^+_{fog, atmos}$ and $CCHO_{fog, atmos}$ by one to three orders of magnitude higher than the atmospheric concentrations in aerosols discussed in section 3.2. This divergence may be explained by the following:

- Fog scavenging is a transfer process of aerosol particles into the liquid phase of fog droplets (Gilardoni et al., 2014). As fog forms and grows, it can capture aerosol particles in the air and increase their concentration within the fog droplets. This could lead to higher atmospheric concentrations of aerosol particle compounds, especially for the water-soluble and hygroscopic ones, inside the fog compared to the surrounding air.

- The activation of aerosol particles to fog droplets is a process dominated by particle size with larger particles tending to activate first. It is conceivable that SSA particles larger than 10 µm, usually few in number, but with a large mass contribution, were available near the sea surface, where sampling occurred. These SSA particles were activated into fog droplets and contributed significantly to the Na$^+$ and CCHO in the fog. In contrast, aerosol sampling was restricted by the Berner impactor's 10 µm diameter cut-off neglecting the larger particles in the consideration.

- The LWC values were not measured but estimated, which could be a source of errors. This approach resulted in values representing rather the upper limit of LWC values typically reported for Arctic summer fog (0.001-0.17 g m^{-3} (Kumai, 1973)) or sea fog (~~However, the calculated LWC values ranged within a realistic frame for Arctic fog~~ 0.02-0.1 g m^{-3} (Herrmann et al., 2015)), but appear within a realistic range. ~~and~~ Consequently, they are likely ~~are~~ not responsible for the large difference between aerosol and fog concentrations ~~in~~ of several orders of magnitude.

22

583 Since both, organic and inorganic constituents, showed higher atmospheric concentrations in
584 fog/clouds compared to ambient aerosol particles, we conclude that a physical phenomenon, such as
585 fog scavenging, might explain this observation and not an in-situ formation within the cloud droplets.
586 Similar to the findings of this study discussing marine CCHO and Na^+ in Arctic fog, Triesch et al. (2021a)
587 found strikingly high concentrations of free amino acids (FAA) and Na^+ in marine clouds compared to
588 aerosol particles both collected on top of the Mt. Verde on Cape Verde as shown in **Table
589 1**.

590 While dFCHO$_{fog}$ and derivatives, such as anhydrosugars and sugar alcohols, have been readily reported
591 for fog water with terrestrial and marine background (Dominutti et al., 2022), we here present for the
592 first time ambient CCHO concentrations in marine fog.

593 **Table 1.** Atmospheric concentrations of selected SSA constituents in fog/clouds compared to ambient aerosol particles during
594 marine field studies.

Chemical constituent	Fog/cloud	PM_{10}	Sampling location	Sampling height	Sampling period	Reference
	(ng m^{-3})	(ng m^{-3})		(m a.s.l.)[h]		
dFCHO	9.2—52[a,b]	—	Reúnion	1760[d]	March—April 2019	Dominutti et al. (2022)
	1.5—1040 (mean:80±260)	<LOD—2.0	Arctic	25[e]	May—July 2017	**this study**
CCHO	3—4300 (mean:390±1100)	0.5—4.7	Arctic	25[e]	May—July 2017	**this study**
FAA	11—490	1.0—4.8	Cape Verde	744[f]	Sept.—Oct. 2017	Triesch et al. (2021a)
	6—79[b]	—	Reúnion	1760[d]	March-April 2019	Dominutti et al. (2022)
	(µg m^{-3})	(µg m^{-3})		(m a.s.l.)[h]		
Na^+	1.6—7.2	0.17—0.40	Cape Verde	744[f]	Sept.—Oct. 2017	Triesch et al. (2021a)
	0.1—2.2[b]	—	Reúnion	1760[d]	March—April 2019	Dominutti et al. (2022)
	0.014—0.063[c]	—	Arctic	180-374[g]	Aug.—Sept. 2018	Zinke et al. (2021)
	0.12—150 (mean:25±43)	0.012—0.77	Arctic	25 m[e]	May—July 2017	**this study**

595 [a]only includes free glucose and rhamnose; sugar alcohols and anhydrosugars were not included for this table. [b]values were
596 calculated from LWCs, molecular weights and concentrations in fog water given within the reference; terrestrial contributions
597 are likely. [c]calculated from concentration in fog water and an assumed LWC of 0.1 g m^{-3}. [d]Piste Omega. [e]RV *Polarstern*. [f]Mt.
598 Verde. [g]tethered balloon. [h]'m a.s.l' abbreviates 'meters above sea level'.

3.4 Chemo-selective sea-air transfer of marine carbohydrates

The chemo-selective sea-air transfer of organics towards inorganic sea salt constituents has been described both in tank and ambient field studies for organic carbon in general (Gantt et al., 2011; Hoffman and Duce, 1976; van Pinxteren et al., 2017) or several chemical constituents, such as carbohydrates (Hasenecz et al., 2020; Schill et al., 2018; Zeppenfeld et al., 2021a), lipids (Triesch et al., 2021b) and free and combined amino acids (Triesch et al., 2021a, c).The calculation of dimensionless ratios between the concentrations of the examined organic parameter and Na^+ allows a comparison of aquatic and atmospheric samples within the marine environment. **Figure 6** Figure 5 shows the $CCHO/Na^+$ ratios for the bulk and SML in the four sea-ice-related sea surface compartments, size resolved aerosol particles and fog water collected during the PS106 cruise.
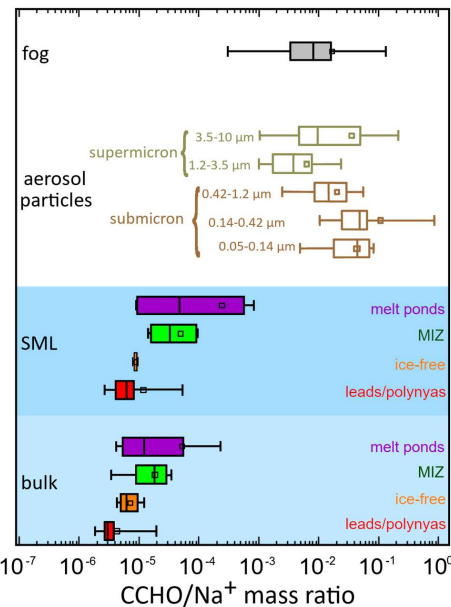
Figure 65. $CCHO/Na^+$ ratios for CCHO in Arctic fog, size-resolved aerosol particles and the surface seawater (SML and bulk) from melt ponds, the marginal ice zone (MIZ), the ice-free ocean and leads/polynyas from the pack ice.

Wide range of $CCHO/Na^+$ ratios in Arctic surface seawater. In the surface seawater samples of this study, the $CCHO/Na^+$ ratios spanned from 2×10^{-6} to 8×10^{-4}, representing a wider range than those found in the Southern Ocean (9×10^{-7} and 3×10^{-5}; Zeppenfeld et al., 2021). While the ratios in the SML and bulk water in general ranged in the same orders of magnitude, large differences were observed in the individual Arctic sea-ice-related sea surface compartments. In the SML, lowest median values were found in the leads/polynyas and ice-free ocean samples with 6×10^{-6} and 9×10^{-6}, respectively, while higher median values appeared in the SML of the MIZ (3×10^{-5}) and melt ponds (4×10^{-5}), or even

24

627   6×10^{-4}, when only aged melt ponds were considered. This large variability of CCHO/Na$^+$ ratios can be

628   explained by the variable content of CCHO (high CCHO content in aged melt ponds & MIZ versus lower

629   CCHO content in ice-free ocean & leads/polynyas) and Na$^+$ (low salinity in the SML of melt ponds versus

630   higher salinities in ice-free ocean & leads/polynyas & MIZ) in the different sea-ice-related sea surface

631   compartments. It can be expected, that the different CCHO/Na$^+$ ratios in the individual seawater

632   compartments impacted the corresponding CCHO/Na$^+$ ratios in fog and aerosol particles during the

633   sea-air transfer, and consequently the enrichment factors for the sea-air transfer (EF$_{aer}$, EF$_{fog}$), which

634   are calculated from those ratios.

635   ***Air mass history influences CCHO$_{aer}$/Na$^+_{aer}$ ratios in Arctic aerosol particles.*** In contrast to the

636   seawater samples, CCHO$_{aer}$/Na$^+_{aer}$ ratios were much higher for aerosol particles considering the size

637   resolution $(1 \times 10^{-3} – 9 \times 10^{-1})$ supporting the concept of the chemo-selective enrichment of

638   carbohydrates towards Na$^+$ during the transfer from the ocean into the atmosphere. In this context,

639   submicron particles showed much higher median ratios of 4×10^{-2} (0.05–0.14 µm) and 4×10^{-2}

640   (0.14–0.42 µm) than supermicron particles with 4×10^{-3} (1.2–3.5 µm) and 1×10^{-2} (3.5–10 µm).

641   ~~Considering~~ Regarding PM$_{10}$ (sum of all five Berner stages), the CCHO$_{aer,PM10}$/Na$^+_{aer,PM10}$ ratios varied

642   much more in the Arctic study presented here $(2 \times 10^{-3} – 2 \times 10^{-1}$, see **Table SI 1** ~~Table SI 1~~) than in the ice-

643   free part of the Southern Ocean $(8 \times 10^{-4} – 7 \times 10^{-3}$; Zeppenfeld et al. (2021b)).

644   During four aerosol sampling periods (24/05/17–26/05/17; 26/05/17–29/05/17; 29/05/17–01/06/17;

645   19/06/17–25/06/17), air masses had predominantly passed over the ice-free ocean (45–100% of the

646   12 hours prior to sampling, as shown in **Table SI 1** & **Figure SI 2**). Interestingly, these periods exhibited

647   the lowest CCHO$_{aer,PM10}$/Na$^+_{aer,PM10}$ ratios $(2 \times 10^{-3} – 9 \times 10^{-3}$, detailed in **Table SI 1**), values that are

648   strikingly similar to those observed in the ice-free Southern Ocean. ~~Interestingly, in the four aerosol~~

649   ~~sampling periods (24/05/17–26/05/17; 26/05/17–29/05/17; 29/05/17–01/06/17;~~

650   ~~19/06/17–25/06/17) where the air masses had passed the majority (45–100%) of the previous 12 h~~

651   ~~before sampling over the open, ice-free ocean (trajectories combined with sea ice maps can be found~~

652   ~~in **Figure SI 3**) exhibited the lowest CCHO$_{aer,PM10}$/Na$^+_{aer,PM10}$ ratios $(2 \times 10^{-3} – 9 \times 10^{-3}$, see **Table SI 1**), very~~

653   ~~similar to the values in the ice-free Southern Ocean.~~ In contrast, higher ratios were found, when the

654   air masses had rested a significant time over the pack ice or the MIZ. This could be an indication that

655   the chemical composition of the sea-ice-related sea surface compartments, here the ice-free ocean

656   with low CCHO/Na$^+$ ratios, strongly influences the relative composition of aerosol particles. In contrast,

657   the influence of the MIZ, pack ice and melt ponds exhibiting quite different chemical, physical and

658   biological properties on CCHO$_{aer,PM10}$/Na$^+_{aer,PM10}$ could not be resolved in further details following this

659   approach using back-trajectory calculations and satellite data. This is certainly due to the proximity of

660   these sea-ice-related sea surface compartments on a small spatial scale (especially melt ponds in

661 direct vicinity to open leads), the long sampling periods of aerosol particles, the lacking knowledge of

662 deposition rates, the effect of wind on wave propagation and bubble bursting processes within the

663 individual sea-ice-related sea surface compartments and missing data on the biological activities in

664 individual melt ponds.

665 ***Similar CCHO/Na$^+$ ratios in aerosol particles and fog.*** For fog, $CCHO_{fog}/Na^+_{fog}$ ratios ranged from

666 3×10^{-4} to 1×10^{-1}, which covers the same orders of magnitude of aerosol particles. Even though absolute

667 atmospheric concentrations of CCHO are much higher in fog than in aerosol particles possibly due to

668 fog scavenging (as discussed in 3.3), the CCHO/Na$^+$ ratios ~~are~~ were similar. This strongly implies that

669 $CCHO_{fog}$ actually originated from the ambient marine aerosol particles. The attempt to find matches or

670 common trends between aerosol particles and the fog in individual samples was not successful,

671 certainly due to the very different resolutions of sampling times and in addition due to the probability

672 of fog droplets containing aerosol particles bigger than 10 μm.

673 ***Calculated EF$_{aer}$ and EF$_{fog}$ depend on the sea-ice-related marine source under consideration.*** EF$_{aer}$ and

674 EF$_{fog}$ are calculated as a quotient between the CCHO/Na$^+$ ratios in the size-resolved aerosol

675 particles/fog and the corresponding bulk water. The CCHO/Na$^+$ ratios ~~concentrations~~ in the Arctic

676 seawater of this study ~~was~~ were very variable depending on the regarded sea-ice-related sea surface

677 compartment environment, as well in the aerosol particles and in fog water. This fact strongly

678 impacted the resulting hypothetical EF$_{aer}$ and EF$_{fog}$, enabling calculated values ranging between 10^1 and

679 10^4 for supermicron aerosol particles, between 10^2 and 10^5 for submicron particles and between 10^0

680 and 10^4 for fog depending on which sea-ice-related sea surface compartment was assumed as the

681 marine source of SSA as shown in **Figure 7**~~Figure 6~~. Due to missing information, including SSA emission

682 fluxes from the four sea-ice-related compartments, aerosol deposition rates, biological activities in

683 melt ponds, wind effects on wave propagation and bubble bursting, and the comparative importance

684 of melt ponds versus open leads (which are in close proximity, making it difficult to resolve them in

685 back-trajectory analyses) as SSA sources – we didn't perform calculations based on the back-trajectory

686 history of each atmospheric sample. Instead, subsequent calculations for EF$_{aer}$ and EF$_{fog}$ employed a

687 hypothetical approach, assessing the range of enrichment factors by considering only one of the four

688 sea-ice-related compartments—represented by the corresponding median $CCHO_{bulk}/Na^+_{bulk}$ ratios—as

689 the only source, while excluding the others.

690 Lower atmospheric EFs were calculated when aged melt ponds (EF$_{aer,super}$=19–750; EF$_{aer,sub}$=127–5100;

691 EF$_{fog}$=5–2400) or the MIZ (EF$_{aer,super}$=60–2310; EF$_{aer,sub}$=390–16000; EF$_{fog}$=17–7400) were assumed as

692 the only (theoretical) ~~marine~~ source of CCHO and Na$^+$, while higher values were found with the ice-

693 free ocean (EF$_{aer,super}$=175–6800; EF$_{aer,sub}$=1100–46000; EF$_{fog}$=50–22000) or open leads/polynyas

694 (EF$_{aer,super}$=360–14000; EF$_{aer,sub}$=2360–95000; EF$_{fog}$=103–44600). It is important to note that EFs were

695 most consistent with results from other CCHO sea-air transfer studies in the tank (Hasenecz et al.,
696 2020) and the field (Zeppenfeld et al., 2021a), when aged melt ponds or the MIZ were considered as
697 the ~~oceanic~~only emission source. If leads/polynyas and the ice-free ocean were~~are~~ regarded as the
698 only emission source, higher EF_{aer} and EF_{fog} values ~~resulted~~were obtained, and hence a possible~~the~~
699 ~~assumption~~ overestimation of the~~a stronger~~ mechanistic process of enrichment. ~~~~As the results on
700 back-trajectory calculations and sea ice maps demonstrated (**Table SI 1** & **Figure SI 2**), most air masses
701 were exposed to several of the sea-ice-related sea surface compartments before sampling~~It is highly~~
702 ~~unlikely whether an air mass package had been exclusively exposed to leads/polynyas during its~~
703 ~~history, and not to aged melt ponds or the MIZ.~~ Consequently, none of the Arctic sea-ice--related sea
704 surface compartments discussed above should be ~~neglected in the~~overlooked when discussing~~on~~ of
705 sea-air transfer of organic substances.

706 During the same Arctic field campaign, Hartmann et al. (2021) investigated INP in ambient aerosol
707 particles and compared it to bulk and SML in seawater from all the different sea-ice--related sea surface
708 compartments using similar EF_{aer} calculations as reported here. They concluded that an enrichment of
709 3 to 5 orders of magnitude was necessary during the sea-air transfer to fully attribute atmospheric INP
710 to oceanic sources. Here, we show that such high EF_{aer} and EF_{fog} for organics, and hence marine
711 biogenic INP, can be calculated, e.g. when open leads/polynyas were referred to as the only oceanic
712 source. In summary, Artic air masses have been impacted by different types of sea-ice--related sea
713 surface compartments before sampling, whereas it is still unclear which one has the biggest effect on
714 the chemical composition of the marine aerosol particles. This aspect should be considered when the
715 marine SSA constituents are modelled for the Arctic from remote sensing data.

Formatiert: Schriftart: Fett

27

716

717

718

719

720

721

722

723

724

725
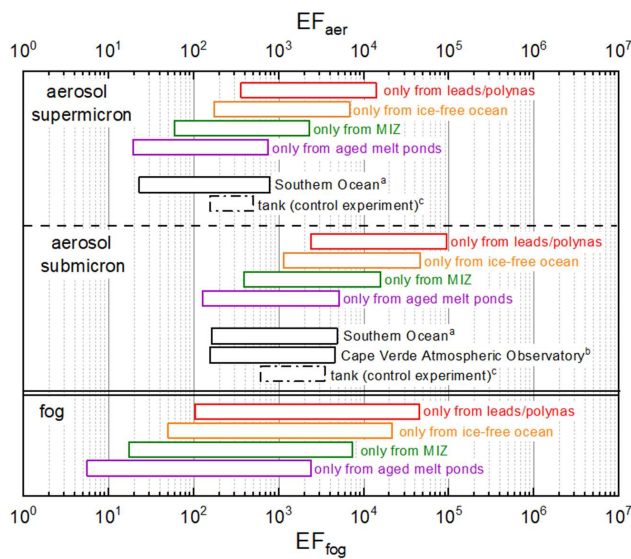
Figure 76. Range of calculated hypothetical enrichment factors EF_{aer} and EF_{fog} assuming either leads/polynyas, the ice-free ocean, the MIZ or aged melt ponds as the only marine source for the sea-air transfer of CCHO in the Arctic. For the calculation of EF_{aer} and EF_{fog}, the minimum and maximum values of the $CCHO_{aer/fog}/Na^+_{aer/fog}$ ratios and the median values of $CCHO_{bulk}/Na^+_{bulk}$ were used. The EF_{aer} values of this study were compared with the results of a) the field study conducted in the Southern Ocean by Zeppenfeld et al. (2021), b) the field study conducted at Cape Verde Atmospheric Observatory (CVAO) by van Pinxteren et al. (2023) and c) the results of the CCHO tank study by Hasenecz et al. (2020) without any addition of heterotrophic bacteria (control experiment). Here, EF_{aer} values were calculated from the experimental data published by Hasenecz et al. (2020b).

726

727

728

729

730

731

732

733

734

735

736

28

737

3.5 Atmospheric aging of marine carbohydrates

To resolve the fate of marine carbohydrates in the atmosphere after their ejection from the ocean, the relative molar contributions of monosaccharides to CCHO were compared between the bulk and SML from the leads/polynyas, MIZ, ice-free ocean and melt pond samples, as well as the sub-and supermicron aerosol particles and fog water (**Figure 8**~~Figure 7~~). The composition of marine carbohydrates in seawater strongly depends on the dominating microbial species, season, diagenetic state, availability of nutrients and environmental stress factors (Engbrodt, 2001; Goldberg et al., 2011) leading to a natural variability among individual samples even within small spatial scales. Consequently, to enable the direct comparison of seawater with atmospheric samples of this field study with an elevated level of statistical certainty, here we compare the mean values of the entire data set, instead of individual samples. Finally, in addition to the changes of the monosaccharide patterns of CCHO, the systematic degradation of CCHO to *d*FCHO was observed in the atmosphere and will be discussed within this ~~chapter~~section.

CCHO composition in different sea-ice--related sea surface compartments and depths is similar. In seawater (bulk and SML), glucose (means= 35–48 mol%), galactose (means= 13–18 mol%) and xylose (means= 7–16 mol%) dominated the CCHO composition followed by smaller contributions of other neutral sugars, amino sugars, uronic acids and muramic acid (**Figure 8**~~Figure 7~~). Considering the natural variability among individual samples, there were no significant differences in means between the bulk and SML, nor between the lead/polynya, MIZ, ice-free ocean and melt pond samples. Variations were observed between the dissolved and particulate fractions (**Figure SI 3**~~Figure SI 6~~), nevertheless the combined carbohydrates within all sea-ice--related sea surface compartments followed the same pattern of the predominance of glucose, galactose and xylose. Overall, the relative monosaccharide compositions of glucose **>** (galactose ≈ xylose) **>** other (neutral or charged) monosaccharides of the seawater samples from this Arctic study appear similar to the monosaccharide compositions investigated in the SML and bulk water from the Central Arctic Ocean (Gao et al., 2012) and at the western Antarctic peninsula (Zeppenfeld et al., 2021a), the meltwater of Arctic multiyear sea ice (Amon et al., 2001) and the epipelagic water from the Ross Sea (Kirchman et al., 2001).

Less galactose, but more muramic acid in atmospheric CCHO$_{aer}$ and CCHO$_{fog}$. Atmospheric samples showed a different monosaccharide pattern within the hydrolyzed CCHO in comparison to the seawater and melt pond samples. While glucose (means= 41 mol% for fog; 50 mol% for submicron and 60 mol% for ~~fog, submicron and~~ supermicron aerosol particles~~, respectively~~) and xylose (means= 16; 15 and 15 mol%) still prevailed over the relative monosaccharide pattern, the contribution of galactose (means= 6; 3 and 3 mol%) was strongly reduced, both in fog and aerosol particles. On the other hand,

30
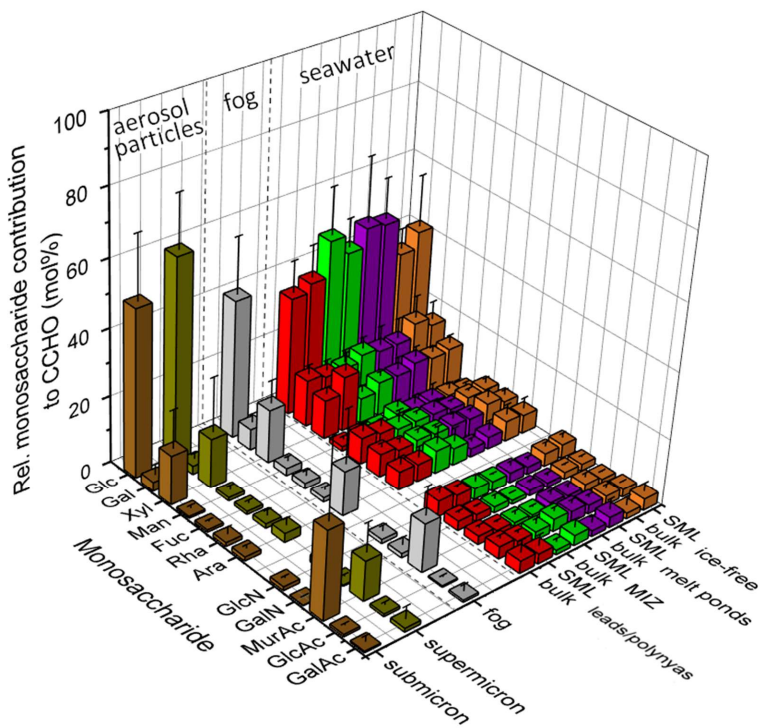
Figure 87. Relative monosaccharide composition of combined carbohydrates (CCHO) after acid hydrolysis in sub-/supermicron aerosol particles, fog water, bulk and SML samples from the leads and polynyas within the pack ice, the MIZ, the ice-free ocean and young and aged melt ponds. The 3D bar chart shows the averages and standard deviations of the relative contributions. Glc: glucose, Gal: galactose, Xyl: xylose, Man: mannose, Fuc: fucose, Ara: arabinose, GlcN: glucosamine, GalN: galactosamine, MurAc: muramic acid, GlcAc: glucuronic acid, GalAc: galacturonic acid.

771 the ratio of muramic acid was strongly elevated in aerosol particles (means= 12 and 26 mol%) and fog

772 water (mean= 14 mol%) in comparison to the oceanic samples (means= 0.9–2.6 mol%). These

773 differences of the relative monosaccharide contributions to CCHO among the seawater and the

774 atmospheric samples described within this study are in good agreement with the sea-air transfer

775 investigations conducted in the Southern Ocean at the western Antarctic peninsula (Zeppenfeld et al.,

776 2021a). Consequently, the occurring phenomenon might be independent from the sampling location

777 and could be explained by three possible atmospheric processes, such as (1) a chemo-selective sea-air

778 transfer of certain oligo- or polysaccharides over others, (2) an atmospheric transformation due to

779 abiotic chemical reactions or (3) an atmospheric transformation due to microbiological activities.

780 Among these possible pathways, Zeppenfeld et al. (2021) presumed the secondary atmospheric

781 transformation caused by microbiological metabolism as the most probable or at least most dominant

782 one supported by the prevalence of muramic acid, an amino sugar acid naturally occurring in bacterial

31

783   cell walls (Mimura and Romano, 1985; Sud and Tyler, 1964), and the very selective absence of certain
784   monosaccharides in the $CCHO_{aer}$ in aerosol particles as it was observed in this Arctic study as well.

785   ***Formation of combined arabinose in fog.*** A comparison of the monosaccharide composition of aerosol
786   particles and fog water showed great similarity regarding dominant contributions from glucose, xylose
787   and muramic acid. It seems plausible that the fog water droplets contained the same inorganic and
788   organic compounds found in the SSA particles assuming that SSA particles activated the formation of
789   fog droplets as CCN due to their rather large diameters and high hygroscopicity. Apart from that,
790   however, a significant difference was observed in the increased relative contribution of arabinose in
791   fog (mean= 13 mol%) compared to aerosol particles (means= 1.2 and 2.7 mol%) indicating a formation
792   of arabinose in the liquid phase. During a marine microcosm experiment performed by Hasenecz et al.
793   (2020), a strong link was observed between the release of arabinose-containing polysaccharides in
794   form of EPS and the presence of heterotrophic bacteria and stressed phytoplankton. Furthermore, a
795   strain of the psychrotolerant marine bacterium *Pseudoalteromonas* sp. has been shown to produce
796   EPS mainly composed from glucose, arabinose and xylose (Casillo et al., 2018; Qin et al., 2007).
797   Consequently, the release of arabinose-containing EPS in fog could be a plausible protection
798   mechanism of microorganisms contained within a droplet against freezing damage under low Arctic
799   temperatures.

800   ***Indication for microbial activities in the atmosphere.*** Intact bacterial cells at atmospheric
801   concentrations between 5×10^2 and 8×10^4 cells m^{-3} for remote marine and ice-covered regions (Šantl-
802   Temkiv et al., 2018; Mayol et al., 2017), cell-bound and free enzymes have been detected in ambient
803   and nascent marine super- and submicron aerosol particles during several field and tank studies (Aller
804   et al., 2005; Hasenecz et al., 2020; Malfatti et al., 2019; Marks et al., 2001; Rastelli et al., 2017; Šantl-
805   Temkiv et al., 2020; Uetake et al., 2020). For surviving in this hostile environment, some of these
806   microbes have developed a remarkable resilience towards extreme environmental stressors, such as
807   high UV radiation, radical exposure, changing osmolarity, freezing temperatures and desiccation. As
808   survival strategies could serve the selective enzymatic consumption of airborne labile carbohydrates
809   explaining the here observed loss of galactose and the persistence of xylose, the ~~formation~~ release of
810   protecting biofilms from EPS, carotenoid pigmentation or the formation of own precipitating
811   hydrometeors by enabling condensation on a surface as a CCN or freezing by IN active surfaces to
812   reduce their atmospheric residence time (Delort et al., 2010; Matulová et al., 2014; Šantl-Temkiv et
813   al., 2020). Consequently, an enzymatic transformation might serve as a plausible explanation for the
814   selective removal of certain monosaccharides within $CCHO_{aer}$ and $CCHO_{fog}$ observed here. However,
815   the survival and the metabolic activity of microorganisms is restricted by the presence of water (Ervens
816   and Amato, 2020; Haddrell and Thomas, 2017) identifying liquid hydrometeors or fresh SSA as the

32

817 most biologically active atmospheric hotspots. In contrast to most of the ambient aerosol particles, fog
818 droplets provide enough water essential for bacterial activities. However, they might freeze under
819 Arctic sub-zero temperatures possibly causing damage to the microbial cells, which might explain an
820 in-situ formation of a protecting biofilm from arabinose-containing EPS. In a previous Arctic study,
821 Orellana et al. (2011) readily detected microgels in aerosol particles, cloud and fog water most likely
822 emitted from the surface water and the SML via bubble bursting. Indications for an in-situ generation
823 of marine microgels in fog water as an additional source to the primary release from the ocean by
824 bubble bursting have been observed by van Pinxteren et al. (2022) in the tropical Atlantic Ocean.

825 The selective sea-air transfer of certain carbohydrates over others and the abiotic degradation as
826 further possible pathways to the biotic transformation of marine $CCHO_{aer}$ have been discussed in detail
827 in Zeppenfeld et al. (2021), but do not appear, based on the current state of knowledge, as likely
828 explanations of the very selective CCHO degradation and formation of other CCHO observed here.
829 More future lab and mesocosm experiments are required to elucidate the contribution of each of these
830 processes. Finally, the similarity ~~of~~ between the carbohydrate composition~~s~~ of fog water and aerosol
831 particles, both two atmospheric compartments collected with different instrumentation, allows to rule
832 out artefacts of the different sampling and extraction techniques as a reason for the observed
833 differences to the seawater.

834 ***Depolymerization of CCHO to dFCHO, seawater versus atmosphere.*** Free glucose, by far the most
835 prevailing monosaccharide among dFCHO in seawater, ranged between 0.6 and 51 µg L^{-1} during the
836 PS106 cruise in the bulk and the SML (Zeppenfeld et al., 2019a). Thus, dFCHO/CHO ratios, meaning the
837 contribution of sugar monomers to all marine carbohydrates measured in this study, varied between
838 1–14% with an average of 5±3%. Conversely, 86–99% (mean: 95±3) of carbohydrates in the bulk and
839 SML of ocean seawater and melt ponds were incorporated into an oligo- or polysaccharidic structure.
840 CCHO can be hydrolyzed to dFCHO either in an acidic environment or enzymatically by heterotrophic
841 bacteria (Arnosti, 2000; Panagiotopoulos and Sempéré, 2005). Seawater from the Arctic Ocean is
842 slightly alkaline with reported pH values between 7.98 and 8.49 (Rérolle et al., 2016; Tynan et al.,
843 2016), while the pH of melt pond water has been observed to be more variable from mildly acidic (6.1)
844 to more alkaline (10.8) (Bates et al., 2014). In agreement with previous findings, the oceanic surface
845 seawater (pH: 7.98–8.66), including the samples from the MIZ, ice-free ocean and open
846 leads/polynyas, and the melt pond samples (pH: 7.26–8.62) were slightly alkaline in this study.
847 Consequently, it is more plausible that the depolymerization of CCHO in seawater can be ascribed to
848 bacterial activities rather than acid hydrolysis. Since dFCHO are readily resorbed by heterotrophic
849 bacteria with high turnover rates (Ittekkot et al., 1981; Kirchman et al., 2001), concentrations of these
850 monosaccharides are rather low in seawater.

33

851 In contrast, in aerosol particles, higher dFCHO/CHO ratios up to 35% occurred in some selected

852 samples, which is much higher than in seawater, suggesting that CCHO might be depolymerized in the

853 atmosphere. SSA particles are known to significantly acidify within minutes after their release due to

854 the uptake of acidic gases, atmospheric aging reactions with sulfuric dioxide and water loss (Angle et

855 al., 2021). In this context, the surface-to-volume ratio determines the efficiency of the acidification

856 effect, which means that it is most pronounced for submicron SSA particles with reported pH values

857 of 1.5–2.6 within a few minutes in a tank study (Angle et al., 2021), and less pronounced for

858 supermicron SSA particles or cloud droplets (Angle et al., 2022). Consequently, it is conceivable that

859 an acid hydrolysis of CCHO$_{aer}$ to monomeric dFCHO$_{aer}$ occurs at the surface or within the bulk of SSA

860 ~~aerosol~~ particles leading to quick atmospheric aging. However, due to analytical constraints, such as

861 the limits of detections (LODs) of the methodology, the dFCHO in size-resolved aerosol particles could

862 not be detected in all samples and the data availability is not strong enough to draw more conclusions

863 for aerosol particles.

864 In fog, where LODs did not represent an issue due to the high concentrations, dFCHO/CHO ratios

865 exceeding those in seawater were also observed~~higher than to seawater occurred~~, ranging from 1-60%

866 (~~1–60%,~~ mean: 27±16%)~~as well~~. The monosaccharide composition of dFCHO$_{fog}$ was primarily made up

867 of glucose, arabinose, fructose, and xylose, with minor contributions from glucosamine, galactose,

868 mannose, rhamnose, and fucose. While dFCHO$_{fog}$ and CCHO$_{fog}$ shared similar dominant

869 monosaccharides, fructose was only present in dFCHO$_{fog}$. This absence in CCHO$_{fog}$ is attributed to

870 fructose's low stability during the analytical preparation for CCHO analysis (Panagiotopoulos and

871 Sempéré, 2005). As a result, fructose won't be further discussed. ~~The monosaccharide composition of~~

872 ~~dFCHO$_{fog}$ was dominated by glucose, arabinose, fructose and xylose with small contributions from~~

873 ~~glucosamine, galactose, mannose, rhamnose and fucose. Consequently, the monosaccharide~~

874 ~~composition of dFCHO$_{fog}$ was quite similar to CCHO$_{fog}$, just with the difference that fructose was~~

875 ~~detected in dFCHO$_{fog}$ but not in CCHO$_{fog}$, which is due to the low stability of fructose towards the~~

876 ~~analytical preparation procedure for the analysis of CCHO (Panagiotopoulos and Sempéré, 2005) and~~

877 ~~should, hence, not find further considerations.~~ In this study, pH values of fog water ranged between

878 5.7 and 6.8, which is 1–2 magnitudes more acidic than in seawater. Polysaccharides are known to

879 depolymerize due to acid hydrolysis, especially at elevated temperatures. The pH-stability can be

880 largely variable among the different polysaccharides; however, we are not aware of studies that have

881 shown such fast depolymerizations, in the sense of time scales relevant for atmospheric lifetime of

882 aerosol particles, at such mildly acid conditions and low temperatures as those of the Arctic

883 atmosphere. Furthermore, there was no significant correlation between the pH and the dFCHO/CHO

884 of these cloud samples. Consequently, there are no indications that the majority of CCHO was

Formatiert: Tiefgestellt

885 hydrolyzed inside the cloud droplets, however it might be conceivable that hydrolysis had readily
886 occurred within the non-activated SSA particle where pH values were much lower.

887 Besides an acid hydrolysis induced by quick atmospheric acidification of SSA particles, atmospheric
888 radicals, such as OH (Trueblood et al., 2019), or photolytic cleavages of glycosidic bonds (Kubota et al.,
889 1976) could have contributed to the degradation of atmospheric CCHO to monomeric dFCHO in SSA
890 and marine fog. For these processes, however, still hardly any systematic lab studies have been
891 conducted for the plurality of marine polysaccharides, which makes a classification of the meaning of
892 these processes difficult. A preferred sea-air transfer of dFCHO over CCHO to explain this observation
893 seems unlikely based on the missing enrichment of neutral dFCHO in contrast to the high EF_{aer} of CCHO
894 shown in tank studies (Hasenecz et al., 2019, 2020). Finally, a microbial depolymerization of CCHO by
895 extracellular enzymes in fog cannot be entirely ruled out considering that the activity of some
896 polysaccharide-degrading enzymes, such as α- and β-glucosidase, have been found to accelerate in
897 seawater with increasing acidity (Piontek et al., 2010). However, this finding was conducted for a pH
898 range only 0.3 pH units lower than the typical pH of seawater and it is not sure, if this finding can be
899 transferred to the more acid conditions in aerosol particles and fog water.

900 ***Several aging processes in the atmosphere.*** We observed significant changes between the chemical
901 composition of marine carbohydrates in the surface seawater, including the bulk and SML, and
902 atmospheric carbohydrates, including aerosol particles and fog. Based on the changing
903 monosaccharide composition pattern of CCHO with selective degradation and formation of specific
904 monosaccharides within CCHO, we conclude microbial or enzymatic activities within the aerosol
905 particles of fog droplets. Furthermore, the increasing contribution of dFCHO to the total carbohydrate
906 pool in fog and aerosol particles might be attributed to a hydrolytic cleavage of the glycosidic linkages
907 between monosaccharide unites within the oligo-and polysaccharides after a quick atmospheric
908 acidification of SSA particles. Consequently, atmospheric carbohydrates experience quick atmospheric
909 aging, potentially due to both biological and abiotic processes, after their release from the ocean.
910 Possibly, this could affect the CCN and INP properties of marine carbohydrates and hence the
911 formation and properties of clouds.

3.6 Perspective assessment of CCHO via bio-optical parameters

The absorption of phytoplankton (a_{ph}) and CDOM (a_{CDOM}) are bio-optical parameters providing additional information about the chemical and microbiological history of the water masses within the particulate and dissolved phase, respectively. They can be measured on discrete water samples and can also be assessed as products from satellites (Lefering et al., 2017; Matsuoka et al., 2012, 2013; Röttgers et al., 2016). Here we tested, if a_{ph} or CDOM parameters correlate with CCHO in seawater to potentially enable the remote-sensing approximation of marine CCHO in seawater and potentially in the atmosphere.

***Good assessment of CCHO in seawater via* $a_{ph}440$**. $a_{ph}440$ derived from the phytoplankton absorption spectrum is directly related to the biomarker TChl-*a* indicating phytoplankton biomass (Bricaud et al., 2004; Phongphattarawat, 2016). The advantage of using $a_{ph}440$ over pigment data, including TChl-*a* from full high-performance liquid chromatography (HPLC) analysis (e.g. Barlow et al., 1997; Taylor et al., 2011), is the lower need of sample volume for the analysis. This allows the determination of values in the SML samples as well (Zäncker et al., 2017), which are laborious to collect and therefore limited in availability. In this study, $a_{ph}440$ strongly correlated with *p*CCHO (R=0.90, p<0.001) in bulk and SML samples (**Figure 9**Figure SI 4a) showing a direct link with fresh phytoplankton biomass production. A similar link has been described before for TChl-*a* and *p*CCHO in the photic layer of the Ross Sea (Fabiano et al., 1993), in the ocean west of the Antarctic peninsula (Zeppenfeld et al., 2021a) and between TChl-*a* and the particulate form of laminarin, an algal polysaccharide, in Arctic and Atlantic water samples (Becker et al., 2020). *d*CCHO showed a good, but weaker correlation with $a_{ph}440$ (R=0.66, p<0.001) than *p*CCHO. This finding supports the assumption that *p*CCHO are rather freshly produced by local autotrophs, while the link between *d*CCHO with their primary production was already ~~contorted~~ obscured by subsequent transformation processes resulting in a more recalcitrant, long-lived mix of macromolecules (Goldberg et al., 2011; Hansell, 2013; Keene et al., 2017). Nevertheless, CCHO, the sum from *d*CCHO and *p*CCHO, showed a high correlation with $a_{ph}440$ (R=0.84, p<0.001, **Figure 9b**) leading to the conclusion that this bio-optical parameter derived from the $a_{ph}(\lambda)$ spectrum is suitable to assess the total amount of CCHO in the surface seawater of the different sea-ice-related sea surface compartments of the Arctic.

***Good assessment of CCHO in seawater via* $a_{CDOM}350$**. In this study, high correlations were observed between *d*CCHO and $a_{CDOM}350$ (R=0.66, p<0.001, **Figure 10**Figure SI 5a), and weaker correlations between *d*CCHO and $a_{CDOM}443$ (R=0.53, p<0.001, **Figure 10**Figure SI 5b). The better correlation at λ=350 nm compared to 443 nm can be explained by the fact that a_{CDOM} exponentially decreases with wavelength. While absorption by CDOM is higher at λ=350 nm, it is much closer to the method

945 detection limit at λ=443 nm and is therefore more error-prone. However, with current satellite

946 products only a_{CDOM} at 440 nm can be retrieved.

947 Previous studies reported strong correlations between $a_{CDOM}350$ and dissolved organic carbon (DOC)

948 in Arctic seawater (Gonçalves-Araujo et al., 2015; Spencer et al., 2009; Stedmon et al., 2011; Walker

949 et al., 2013). Consequently, it is conceivable that dCCHO, an important constituent of DOC, shows good

950 correlations as well. Surprisingly, the correlation between CCHO (sum of dCCHO and pCCHO) and

951 $a_{CDOM}350$ was strongest (R=0.85, p<0.001, **Figure 10**~~Figure SI 5~~c), indicating that CDOM retrieval from

952 high-resolution satellite data could allow a good approximation of CCHO in Arctic seawater.

953
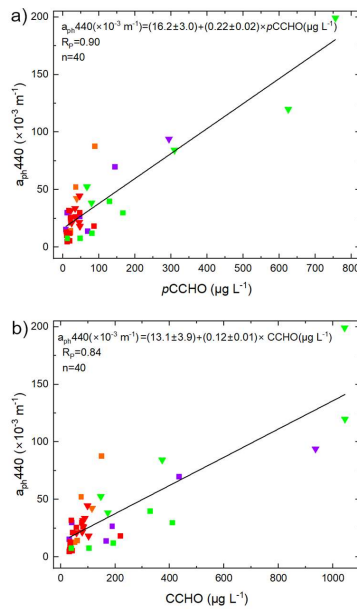
967 **Figure 9.** Correlation plots of $a_{ph}440$ derived from PAB spectra against a) pCCHO and b) CCHO. Triangles: SML, squares: bulk. Green: marginal ice zone (MIZ), purple: melt ponds, orange: ice-free ocean, red: open leads/polynyas in the pack ice.

968

969

970

971

972

973

37

974
975
976
977
978
979
980
981
982
983
984
985
986
987
988
989
990
991

a)
$a_{CDOM}350(\times10^{-3}\,m^{-1})=(100\pm19)+(1.0\pm0.1)\times d CCHO(\mu g\,L^{-1})$
$R_p=0.66$
n=66

b)
$a_{CDOM}443(\times10^{-3}\,m^{-1})=(15\pm2)+(0.07\pm0.01)\times d CCHO(\mu g\,L^{-1})$
$R_p=0.53$
n=66

c)
$a_{CDOM}350(\times10^{-3}\,m^{-1})=(89\pm13)+(0.56\pm0.04)\times CCHO(\mu g\,L^{-1})$
$R_p=0.85$
n=66
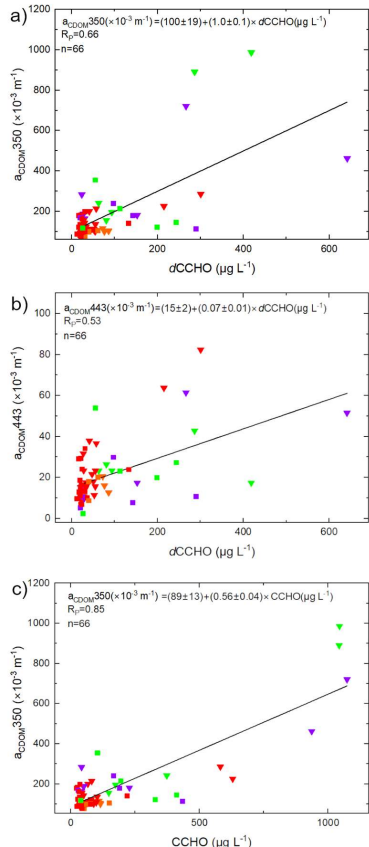
Figure 10. Correlation plots of a) $a_{CDOM}350$ against dCCHO, b) $a_{CDOM}443$ against dCCHO and c) $a_{CDOM}350$ against CCHO. Triangles: SML, squares: bulk. Green: marginal ice zone (MIZ), purple: melt ponds, orange: ice-free ocean, red: open leads/polynyas in the pack ice.

Formatiert: Schriftart: Fett, Nicht Kursiv, Schriftfarbe: Automatisch

Formatiert: Beschriftung, Block

Formatiert: Schriftart: Fett, Nicht Kursiv, Schriftfarbe: Automatisch

Formatiert: Schriftfarbe: Automatisch

4. Summary and Atmospheric Implications

We studied the sea-air transfer of marine carbohydrates from field samples collected in the Arctic during the PS106 campaign from May to July 2017. Large differences of absolute CCHO concentrations and SML enrichments were observed among the different sea-ice-related sea surface compartments (leads/polynyas within the pack ice, ice-free ocean, MIZ, melt ponds). $CCHO_{aer}$ were detected in the sub- and supermicron aerosol particles with indications for primary emissions from the sea through bubble bursting, though the correlations with the SSA tracer Na^+ and wind speed were possibly reduced due to the presence of sea ice influencing the wind-induced SSA emission mechanisms. Atmospheric CCHO and Na^+ concentrations in fog strongly exceeded those of the aerosol particles, likely due to a physical phenomenon. A large enrichment of CCHO in aerosol and fog compared to bulk seawater was observed. The extent of these enrichments varied based on the type of sea-ice-related sea surface compartment assumed as the oceanic source for atmospheric CCHO. We observed a subsequent atmospheric aging of CCHO in the atmosphere, both in aerosol particles and fog, noticed by the selective loss and formation of certain monosaccharide units within CCHO suggesting selective enzymatic/microbial activities, and a depolymerization of CCHO to dFCHO, most measurable in fog water and likely due to abiotic degradation, e.g. acid hydrolysis. CCHO correlated well with bio-optical parameters, such as $a_{ph}440$ from phytoplankton absorption and $a_{CDOM}350$. These parameters can be measured via remote sensing and may allow the retrieval of CCHO from satellite data, which potentially will enable an accurate modelling of atmospheric CCHO concentrations as soon as all emission and atmospheric aging processes are sufficiently understood. This study shows that the Arctic is a complex environment, where the diversity of sea-ice-related sea surface compartments needs to be considered as primary sources of marine CCHO or other organic compounds, and where these molecules can be transformed after their primary sea-air transfer by biological and abiotic processes in the atmosphere.

Marine carbohydrates are assumed to impact cloud properties by acting as CCN and INP (Alpert et al. 2022; Leck et al., 2013; Orellana et al., 2011; van Pinxteren et al., 2022). Studying the chemical identity of those atmospheric nucleation particles, their emission mechanisms and their transformation due to atmospheric aging can strongly improve the understanding of the cloud formation in the Arctic, cloud microphysical properties, the radiation budget, cryosphere-ocean-atmosphere interactions and eventually feedback mechanisms in the frame of Arctic amplification. It can be assumed that within the warming Arctic, where sea ice extent is continuously shrinking, the MIZ area will expand (Strong and Rigor, 2013) and the number of biologically-active melt ponds will increase during the summer

season in the next years. These new MIZ regions and melt ponds could potentially produce more marine carbohydrates than the ice-free ocean or open leads within the pack ice leading to enhanced CCN and INP populations in the Arctic atmosphere serving as a still not well-explored feedback mechanism within Arctic amplification.

Author contribution. SZ wrote the manuscript with contributions from MvP, MH, MZ, AB and HH. SZ, MvP and MH collected the field samples during the PS106 campaign. SZ performed the laboratory carbohydrate analysis and statistical evaluation. MZ and AB assessed the bio-optical parameters. All co-authors proofread and commented the manuscript.

Competing interests. The authors declare that they have no conflict of interest.

List of abbreviations

a_{CDOM} absorption coefficient by colored dissolved organic carbon
aer   aerosol particles

1059	a_{NAP}	absorption coefficient by non-algal particles
1060	ANOVA	Analysis of Variance
1061	a_p	absorption coefficient by total particles
1062	a_{ph}	absorption coefficient by phytoplankton
1063	Ara	arabinose
1064	atmos	atmospheric concentrations
1065	C-CCHO	carbon contained within the combined carbohydrate
1066	CCHO	combined carbohydrates
1067	CCN	cloud condensation nuclei
1068	CDOM	colored dissolved organic matter
1069	CHO	carbohydrates
1070	*d*CCHO	dissolved combined carbohydrates
1071	*d*FCHO	dissolved free carbohydrates
1072	EF	enrichment factor
1073	EPS	exopolymeric substances
1074	ERDDAP	Environmental Research Division's Data Access Program
1075	FAA	free amino acids
1076	Fru	fructose
1077	Fuc	fucose
1078	Gal	galactose
1079	GalN	galactosamine
1080	GalAc	galacturonic acid
1081	Glc	glucose
1082	GlcAc	glucuronic acid
1083	GlcN	glucosamine
1084	HPAEC-PAD	high-performance anion-exchange chromatography with pulsed amperometric detection
1085	HPLC	high-performance liquid chromatography
1086	INP	ice nucleating particles
1087	LWCC	liquid waveguide capillary cell
1088	Man	mannose
1089	MIZ	marginal ice zone
1090	MurAc	muramic acid
1091	Na^+	sodium ion
1092	NOAA	National Oceanic and Atmospheric Administration
1093	OC	organic carbon
1094	OM	organic matter
1095	PAB	particulate absorption
1096	*p*CCHO	particulate combined carbohydrates
1097	PM	particulate matter
1098	Rha	rhamnose
1099	SML	sea surface microlayer
1100	SSA	sea spray aerosol
1101	sub	submicron
1102	super	supermicron
1103	TChl-*a*	total chlorophyll *a*
1104	TEP	transparent exopolymer particles
1105	QFT-ICAM	quantitative filtration technique with an integrative-cavity absorption meter setup
1106	Xyl	xylose

References

Alderkamp, A.-C., Buma, A. G. J., and van Rijssel, M.: The carbohydrates of Phaeocystis and their degradation in the microbial food web, Biogeochemistry, 83, 99–118, https://doi.org/10.1007/s10533-007-9078-2, 2007.

Aller, J. Y., Kuznetsova, M. R., Jahns, C. J., and Kemp, P. F.: The sea surface microlayer as a source of viral and bacterial enrichment in marine aerosols, Journal of Aerosol Science, 36, 801–812, https://doi.org/10.1016/j.jaerosci.2004.10.012, 2005.

Aller, J. Y., Radway, J. C., Kilthau, W. P., Bothe, D. W., Wilson, T. W., Vaillancourt, R. D., Quinn, P. K., Coffman, D. J., Murray, B. J., and Knopf, D. A.: Size-resolved characterization of the polysaccharidic and proteinaceous components of sea spray aerosol, Atmospheric Environment, 154, 331–347, https://doi.org/10.1016/j.atmosenv.2017.01.053, 2017.

Alpert, P. A., Kilthau, W. P., O'Brien, R. E., Moffet, R. C., Gilles, M. K., Wang, B., Laskin, A., Aller, J. Y., and Knopf, D. A.: Ice-nucleating agents in sea spray aerosol identified and quantified with a holistic multimodal freezing model, Science Advances, 8, eabq6842, https://doi.org/10.1126/sciadv.abq6842, 2022.

Álvarez, E., Losa, S. N., Bracher, A., Thoms, S., and Völker, C.: Phytoplankton Light Absorption Impacted by Photoprotective Carotenoids in a Global Ocean Spectrally-Resolved Biogeochemistry Model, Journal of Advances in Modeling Earth Systems, 14, e2022MS003126, https://doi.org/10.1029/2022MS003126, 2022.

Amon, R. M. W., Fitznar, H.-P., and Benner, R.: Linkages among the bioreactivity, chemical composition, and diagenetic state of marine dissolved organic matter, Limnology and Oceanography, 46, 287–297, 2001.

Angle, K., Grassian, V. H., and Ault, A. P.: The rapid acidification of sea spray aerosols, Physics today, 75, https://doi.org/10.1063/PT.3.4926, 2022.

Angle, K. J., Crocker, D. R., Simpson, R. M. C., Mayer, K. J., Garofalo, L. A., Moore, A. N., Garcia, S. L. M., Or, V. W., Srinivasan, S., Farhan, M., Sauer, J. S., Lee, C., Pothier, M. A., Farmer, D. K., Martz, T. R., Bertram, T. H., Cappa, C. D., Prather, K. A., and Grassian, V. H.: Acidity across the interface from the ocean surface to sea spray aerosol, PNAS, 118, https://doi.org/10.1073/pnas.2018397118, 2021.

Arnosti, C.: Substrate specificity in polysaccharide hydrolysis: Contrasts between bottom water and sediments, Limnology and Oceanography, 45, 1112–1119, https://doi.org/10.4319/lo.2000.45.5.1112, 2000.

Aslam, S. N., Michel, C., Niemi, A., and Underwood, G. J. C.: Patterns and drivers of carbohydrate budgets in ice algal assemblages from first year Arctic sea ice, Limnology and Oceanography, 61, 919–937, https://doi.org/10.1002/lno.10260, 2016.

Azetsu-Scott, K. and Passow, U.: Ascending marine particles: Significance of transparent exopolymer particles (TEP) in the upper ocean, Limnology and Oceanography, 49, 741–748, https://doi.org/10.4319/lo.2004.49.3.0741, 2004.

Barlow, R., Cummings, D., and Gibb, S.: Improved resolution of mono- and divinyl chlorophylls a and b and zeaxanthin and lutein in phytoplankton extracts using reverse phase C-8 HPLC, Marine Ecology Progress Series, 161, 303–307, https://doi.org/10.3354/meps161303, 1997.

Barthel, S., Tegen, I., and Wolke, R.: Do new sea spray aerosol source functions improve the results of a regional aerosol model?, Atmospheric Environment, 198, 265–278, https://doi.org/10.1016/j.atmosenv.2018.10.016, 2019.

Bates, N. R., Garley, R., Frey, K. E., Shake, K. L., and Mathis, J. T.: Sea-ice melt CO_2–carbonate chemistry in the western Arctic Ocean: meltwater contributions to air–sea CO_2 gas exchange, mixed-layer properties and rates of net community production under sea ice, Biogeosciences, 11, 6769–6789, https://doi.org/10.5194/bg-11-6769-2014, 2014.

Becker, S., Tebben, J., Coffinet, S., Wiltshire, K., Iversen, M. H., Harder, T., Hinrichs, K.-U., and Hehemann, J.-H.: Laminarin is a major molecule in the marine carbon cycle, PNAS, 117, 6599–6607, https://doi.org/10.1073/pnas.1917001117, 2020.

Benner, R. and Kaiser, K.: Abundance of amino sugars and peptidoglycan in marine particulate and dissolved organic matter, Limnology and Oceanography, 48, 118–128, https://doi.org/10.4319/lo.2003.48.1.0118, 2003.

Bigg, E. K. and Leck, C.: The composition of fragments of bubbles bursting at the ocean surface, Journal of Geophysical Research: Atmospheres, 113, https://doi.org/10.1029/2007JD009078, 2008.

Bikerman, J. J.: Foams, Springer Science & Business Media, 344 pp., 2013.

Bozem, H., Hoor, P., Kunkel, D., Köllner, F., Schneider, J., Herber, A., Schulz, H., Leaitch, W. R., Aliabadi, A. A., Willis, M. D., Burkart, J., and Abbatt, J. P. D.: Characterization of transport regimes and the polar dome during Arctic spring and summer using in situ aircraft measurements, Atmospheric Chemistry and Physics, 19, 15049–15071, https://doi.org/10.5194/acp-19-15049-2019, 2019.

Bricaud, A., Claustre, H., Ras, J., and Oubelkheir, K.: Natural variability of phytoplanktonic absorption in oceanic waters: Influence of the size structure of algal populations, Journal of Geophysical Research: Oceans, 109, https://doi.org/10.1029/2004JC002419, 2004.

Burrows, S. M., Ogunro, O., Frossard, A., Russell, L. M., Rasch, P. J., and Elliott, S.: A Physically Based Framework for Modelling the Organic Fractionation of Sea Spray Aerosol from Bubble Film Langmuir Equilibria, Atmospheric Chemistry and Physics, 14(24):13601–13629, https://doi.org/10.5194/acp-14-13601-2014, 2014.

Burrows, S. M., Gobrogge, E., Fu, L., Link, K., Elliott, S. M., Wang, H., and Walker, R.: OCEANFILMS-2: Representing coadsorption of saccharides in marine films and potential impacts on modeled marine aerosol chemistry, Geophysical Research Letters, 43, 8306–8313, https://doi.org/10.1002/2016GL069070, 2016.

Callaghan, A. H., Deane, G. B., Stokes, M. D., and Ward, B.: Observed variation in the decay time of oceanic whitecap foam, Journal of Geophysical Research: Oceans, 117, https://doi.org/10.1029/2012JC008147, 2012.

Casillo, A., Lanzetta, R., Parrilli, M., and Corsaro, M. M.: Exopolysaccharides from Marine and Marine Extremophilic Bacteria: Structures, Properties, Ecological Roles and Applications, Marine Drugs, 16, 69, https://doi.org/10.3390/md16020069, 2018.

Chen, Q., Mirrielees, J. A., Thanekar, S., Loeb, N. A., Kirpes, R. M., Upchurch, L. M., Barget, A. J., Lata, N. N., Raso, A. R. W., McNamara, S. M., China, S., Quinn, P. K., Ault, A. P., Kennedy, A., Shepson, P. B., Fuentes, J. D., and Pratt, K. A.: Atmospheric particle abundance and sea salt aerosol observations in the springtime Arctic: a focus on blowing snow and leads, Atmospheric Chemistry and Physics, 22, 15263–15285, https://doi.org/10.5194/acp-22-15263-2022, 2022.

Chi, J. W., Li, W. J., Zhang, D. Z., Zhang, J. C., Lin, Y. T., Shen, X. J., Sun, J. Y., Chen, J. M., Zhang, X. Y., Zhang, Y. M., and Wang, W. X.: Sea salt aerosols as a reactive surface for inorganic and organic acidic gases in the Arctic troposphere, Atmospheric Chemistry and Physics, 15, 11341–11353, https://doi.org/10.5194/acp-15-11341-2015, 2015.

Creamean, J. M., Barry, K., Hill, T. C. J., Hume, C., DeMott, P. J., Shupe, M. D., Dahlke, S., Willmes, S., Schmale, J., Beck, I., Hoppe, C. J. M., Fong, A., Chamberlain, E., Bowman, J., Scharien, R., and Persson, O.: Annual cycle observations of aerosols capable of ice formation in central Arctic clouds, Nat Commun, 13, 3537, https://doi.org/10.1038/s41467-022-31182-x, 2022.

Cunliffe, M., Engel, A., Frka, S., Gašparović, B., Guitart, C., Murrell, J. C., Salter, M., Stolle, C., Upstill-Goddard, R., and Wurl, O.: Sea surface microlayers: A unified physicochemical and biological perspective of the air–ocean interface, Progress in Oceanography, 109, 104–116, https://doi.org/10.1016/j.pocean.2012.08.004, 2013.

Cunliffe, M. and Wurl, O.: Guide to best practices to study the ocean's surface., Marine Biological Association of the United Kingdom for SCOR, 2014.

Delort, A.-M., Vaïtilingom, M., Amato, P., Sancelme, M., Parazols, M., Mailhot, G., Laj, P., and Deguillaume, L.: A short overview of the microbial population in clouds: Potential roles in atmospheric chemistry and nucleation processes, Atmospheric Research, 98, 249–260, https://doi.org/10.1016/j.atmosres.2010.07.004, 2010.

DeMott, P. J., Hill, T. C. J., McCluskey, C. S., Prather, K. A., Collins, D. B., Sullivan, R. C., Ruppel, M. J., Mason, R. H., Irish, V. E., Lee, T., Hwang, C. Y., Rhee, T. S., Snider, J. R., McMeeking, G. R., Dhaniyala, S., Lewis, E. R., Wentzell, J. J. B., Abbatt, J., Lee, C., Sultana, C. M., Ault, A. P., Axson, J. L., Martinez, M. D., Venero, I., Santos-Figueroa, G., Stokes, M. D., Deane, G. B., Mayol-Bracero, O. L., Grassian, V. H., Bertram, T. H., Bertram, A. K., Moffett, B. F., and Franc, G. D.: Sea spray aerosol as a unique source of ice nucleating particles, PNAS, 113, 5797–5803, https://doi.org/10.1073/pnas.1514034112, 2016.

Demoz, B. B., Collett, J. L., and Daube, B. C.: On the Caltech Active Strand Cloudwater Collectors, Atmospheric Research, 41, 47–62, https://doi.org/10.1016/0169-8095(95)00044-5, 1996.

Dominutti, P. A., Renard, P., Vaïtilingom, M., Bianco, A., Baray, J.-L., Borbon, A., Bourianne, T., Burnet, F., Colomb, A., Delort, A.-M., Duflot, V., Houdier, S., Jaffrezo, J.-L., Joly, M., Leremboure, M., Metzger, J.-M., Pichon, J.-M., Ribeiro, M., Rocco, M., Tulet, P., Vella, A., Leriche, M., and Deguillaume, L.: Insights into tropical cloud chemistry in Réunion (Indian Ocean): results from the BIO-MAÏDO campaign, Atmospheric Chemistry and Physics, 22, 505–533, https://doi.org/10.5194/acp-22-505-2022, 2022.

Engbrodt, R.: Biogeochemistry of dissolved carbohydrates in the Arctic, Berichte zur Polar-und Meeresforschung (Reports on Polar and Marine Research), 396, 106pp, 2001.

Engel, A. and Händel, N.: A novel protocol for determining the concentration and composition of sugars in particulate and in high molecular weight dissolved organic matter (HMW-DOM) in seawater, Marine Chemistry, 127, 180–191, https://doi.org/10.1016/j.marchem.2011.09.004, 2011.

Engel, A., Bange, H. W., Cunliffe, M., Burrows, S. M., Friedrichs, G., Galgani, L., Herrmann, H., Hertkorn, N., Johnson, M., Liss, P. S., Quinn, P. K., Schartau, M., Soloviev, A., Stolle, C., Upstill-Goddard, R. C., van Pinxteren, M., and Zäncker, B.: The Ocean's Vital Skin: Toward an Integrated Understanding of the Sea Surface Microlayer, Front. Mar. Sci., 4, 165, https://doi.org/10.3389/fmars.2017.00165, 2017.

Ervens, B. and Amato, P.: The global impact of bacterial processes on carbon mass, Atmospheric Chemistry & Physics, 20, 1777–1794, https://doi.org/10.5194/acp-20-1777-2020, 2020.

Fabiano, M., Povero, P., and Danovaro, R.: Distribution and composition of particulate organic matter in the Ross Sea (Antarctica), Polar Biol, 13, 525–533, https://doi.org/10.1007/BF00236394, 1993.

Facchini, M. C., Rinaldi, M., Decesari, S., Carbone, C., Finessi, E., Mircea, M., Fuzzi, S., Ceburnis, D., Flanagan, R., Nilsson, E. D., Leeuw, G. de, Martino, M., Woeltjen, J., and O'Dowd, C. D.: Primary submicron marine aerosol dominated by insoluble organic colloids and aggregates, Geophysical Research Letters, 35, https://doi.org/10.1029/2008GL034210, 2008.

Galgani, L., Piontek, J., and Engel, A.: Biopolymers form a gelatinous microlayer at the air-sea interface when Arctic sea ice melts, Scientific Reports, 6, 29465, https://doi.org/10.1038/srep29465, 2016.

Gantt, B., Meskhidze, N., Facchini, M. C., Rinaldi, M., Ceburnis, D., and O'Dowd, C. D.: Wind speed dependent size-resolved parameterization for the organic mass fraction of sea spray aerosol, Atmospheric Chemistry and Physics, 11, 8777–8790, https://doi.org/10.5194/acp-11-8777-2011, 2011.

Gao, Q., Leck, C., Rauschenberg, C., and Matrai, P. A.: On the chemical dynamics of extracellular polysaccharides in the high Arctic surface microlayer, Ocean Science, 8, 401–418, 2012.

Gilardoni, S., Massoli, P., Giulianelli, L., Rinaldi, M., Paglione, M., Pollini, F., Lanconelli, C., Poluzzi, V., Carbone, S., Hillamo, R., Russell, L. M., Facchini, M. C., and Fuzzi, S.: Fog scavenging of organic and inorganic aerosol in the Po Valley, Atmospheric Chemistry and Physics, 14, 6967–6981, https://doi.org/10.5194/acp-14-6967-2014, 2014.

Goldberg, S. J., Carlson, C. A., Brzezinski, M., Nelson, N. B., and Siegel, D. A.: Systematic removal of neutral sugars within dissolved organic matter across ocean basins, Geophysical Research Letters, 38, https://doi.org/10.1029/2011GL048620, 2011.

Gonçalves-Araujo, R., Stedmon, C. A., Heim, B., Dubinenkov, I., Kraberg, A., Moiseev, D., and Bracher, A.: From Fresh to Marine Waters: Characterization and Fate of Dissolved Organic Matter in the Lena River Delta Region, Siberia, Frontiers in Marine Science, 2, 2015.

Gong, X., Zhang, J., Croft, B., Yang, X., Frey, M. M., Bergner, N., Chang, R. Y.-W., Creamean, J. M., Kuang, C., Martin, R. V., Ranjithkumar, A., Sedlacek, A. J., Uin, J., Willmes, S., Zawadowicz, M. A., Pierce, J. R., Shupe, M. D., Schmale, J., and Wang, J.: Arctic warming by abundant fine sea salt aerosols from blowing snow, Nat. Geosci., 16, 768–774, https://doi.org/10.1038/s41561-023-01254-8, 2023.

Grythe, H., Ström, J., Krejci, R., Quinn, P., and Stohl, A.: A review of sea-spray aerosol source functions using a large global set of sea salt aerosol concentration measurements, Atmospheric Chemistry and Physics, 14, 1277–1297, https://doi.org/10.5194/acp-14-1277-2014, 2014.

Haddrell, A. E. and Thomas, R. J.: Aerobiology: Experimental Considerations, Observations, and Future Tools, Appl. Environ. Microbiol., 83, https://doi.org/10.1128/AEM.00809-17, 2017.

Hansell, D. A.: Recalcitrant Dissolved Organic Carbon Fractions, Annual Review of Marine Science, 5, 421–445, https://doi.org/10.1146/annurev-marine-120710-100757, 2013.

Hara, K., Yamagata, S., Yamanouchi, T., Sato, K., Herber, A., Iwasaka, Y., Nagatani, M., and Nakata, H.: Mixing states of individual aerosol particles in spring Arctic troposphere during ASTAR 2000 campaign, Journal of Geophysical Research: Atmospheres, 108, https://doi.org/10.1029/2002JD002513, 2003.

Hartmann, M., Gong, X., Kecorius, S., van Pinxteren, M., Vogl, T., Welti, A., Wex, H., Zeppenfeld, S., Herrmann, H., Wiedensohler, A., and Stratmann, F.: Terrestrial or marine – indications towards the origin of ice-nucleating particles during melt season in the European Arctic up to 83.7° N, Atmospheric Chemistry and Physics, 21, 11613–11636, https://doi.org/10.5194/acp-21-11613-2021, 2021.

Hasenecz, E., Jayarathne, T., Pendergraft, M. A., Santander, M. V., Mayer, K. J., Sauer, J., Lee, C., Gibson, W. S., Kruse, S. M., Malfatti, F., Prather, K. A., and Stone, E. A.: Marine bacteria affect saccharide enrichment in sea spray aerosol during a phytoplankton bloom, ACS Earth Space Chem., 4, 1638–1649, https://doi.org/10.1021/acsearthspacechem.0c00167, 2020.

Hasenecz, E. S., Kaluarachchi, C. P., Lee, H. D., Tivanski, A. V., and Stone, E. A.: Saccharide Transfer to Sea Spray Aerosol Enhanced by Surface Activity, Calcium, and Protein Interactions, ACS Earth Space Chem., 3, 2539–2548, https://doi.org/10.1021/acsearthspacechem.9b00197, 2019.

Held, A., Brooks, I. M., Leck, C., and Tjernström, M.: On the potential contribution of open lead particle emissions to the central Arctic aerosol concentration, Atmospheric Chemistry and Physics, 11, 3093–3105, https://doi.org/10.5194/acp-11-3093-2011, 2011.

Herrmann, H., Schaefer, T., Tilgner, A., Styler, S. A., Weller, C., Teich, M., and Otto, T.: Tropospheric Aqueous-Phase Chemistry: Kinetics, Mechanisms, and Its Coupling to a Changing Gas Phase, Chem. Rev., 115, 4259–4334, https://doi.org/10.1021/cr500447k, 2015.

Hoffman, E. J. and Duce, R. A.: Factors influencing the organic carbon content of marine aerosols: A laboratory study, Journal of Geophysical Research (1896-1977), 81, 3667–3670, https://doi.org/10.1029/JC081i021p03667, 1976.

44

Huang, J. and Jaeglé, L.: Wintertime enhancements of sea salt aerosol in polar regions consistent with a sea ice source from blowing snow, Atmos. Chem. Phys., 17, 3699–3712, https://doi.org/10.5194/acp-17-3699-2017, 2017.

Istomina, L.: Retrieval of Sea Ice Surface Melt Using OLCI Data Onboard Sentinel-3, 2020, C017-07, 2020.

Ittekkot, V., Brockmann, U., Michaelis, W., and Degens, E. T.: Dissolved free and combined carbohydrates during a phytoplankton bloom in the northern North Sea, Marine Ecology Progress Series, 4, 299–305, 1981.

Karl, M., Leck, C., Rad, F. M., Bäcklund, A., Lopez-Aparicio, S., and Heintzenberg, J.: New insights in sources of the sub-micrometre aerosol at Mt. Zeppelin observatory (Spitsbergen) in the year 2015, Tellus B: Chemical and Physical Meteorology, 71, 1613143, https://doi.org/10.1080/16000889.2019.1613143, 2019.

Kecorius, S., Vogl, T., Paasonen, P., Lampilahti, J., Rothenberg, D., Wex, H., Zeppenfeld, S., van Pinxteren, M., Hartmann, M., Henning, S., Gong, X., Welti, A., Kulmala, M., Stratmann, F., Herrmann, H., and Wiedensohler, A.: New particle formation and its effect on cloud condensation nuclei abundance in the summer Arctic: a case study in the Fram Strait and Barents Sea, Atmospheric Chemistry and Physics, 19, 14339–14364, https://doi.org/10.5194/acp-19-14339-2019, 2019.

Keene, W. C., Long, M. S., Reid, J. S., Frossard, A. A., Kieber, D. J., Maben, J. R., Russell, L. M., Kinsey, J. D., Quinn, P. K., and Bates, T. S.: Factors That Modulate Properties of Primary Marine Aerosol Generated From Ambient Seawater on Ships at Sea, Journal of Geophysical Research: Atmospheres, 122, 11,961-11,990, https://doi.org/10.1002/2017JD026872, 2017.

Kirchman, D. L., Meon, B., Ducklow, H. W., Carlson, C. A., Hansell, D. A., and Steward, G. F.: Glucose fluxes and concentrations of dissolved combined neutral sugars (polysaccharides) in the Ross Sea and Polar Front Zone, Antarctica, Deep Sea Research Part II: Topical Studies in Oceanography, 48, 4179–4197, https://doi.org/10.1016/S0967-0645(01)00085-6, 2001.

Kirpes, R. M., Bondy, A. L., Bonanno, D., Moffet, R. C., Wang, B., Laskin, A., Ault, A. P., and Pratt, K. A.: Secondary sulfate is internally mixed with sea spray aerosol and organic aerosol in the winter Arctic, Atmos. Chem. Phys., 18, 3937–3949, https://doi.org/10.5194/acp-18-3937-2018, 2018.

Krembs, C. and Deming, J. W.: The role of exopolymers in microbial adaptation to sea ice, in: Psychrophiles: from biodiversity to biotechnology, Springer, 247–264, 2008.

Krembs, C., Eicken, H., Junge, K., and Deming, J. W.: High concentrations of exopolymeric substances in Arctic winter sea ice: implications for the polar ocean carbon cycle and cryoprotection of diatoms, Deep Sea Research Part I: Oceanographic Research Papers, 49, 2163–2181, https://doi.org/10.1016/S0967-0637(02)00122-X, 2002.

Kubota, H., Ogiwara, Y., and Matsuzaki, K.: Photo-Induced Formation of Peroxide in Saccharides and Related Compounds, Polymer Journal, 8, 557–563, https://doi.org/10.1295/polymj.8.557, 1976.

Kumai, M.: Arctic Fog Droplet Size Distribution and Its Effect on Light Attenuation, Journal of the Atmospheric Sciences, 30, 635–643, https://doi.org/10.1175/1520-0469(1973)030<0635:AFDSDA>2.0.CO;2, 1973.

Lawler, M. J., Saltzman, E. S., Karlsson, L., Zieger, P., Salter, M., Baccarini, A., Schmale, J., and Leck, C.: New Insights Into the Composition and Origins of Ultrafine Aerosol in the Summertime High Arctic, Geophysical Research Letters, 48, e2021GL094395, https://doi.org/10.1029/2021GL094395, 2021.

Leck, C.: Chemical composition and sources of the high Arctic aerosol relevant for cloud formation, Journal of Geophysical Research, 107, https://doi.org/10.1029/2001JD001463, 2002.

Leck, C., Gao, Q., Mashayekhy Rad, F., and Nilsson, U.: Size-resolved atmospheric particulate polysaccharides in the high summer Arctic, Atmospheric Chemistry and Physics, 13, 12573–12588, https://doi.org/10.5194/acp-13-12573-2013, 2013.

Lefering, I., Röttgers, R., Utschig, C., and McKee, D.: Uncertainty budgets for liquid waveguide CDOM absorption measurements, Appl. Opt., AO, 56, 6357–6366, https://doi.org/10.1364/AO.56.006357, 2017.

Liu, Y., Röttgers, R., Ramírez-Pérez, M., Dinter, T., Steinmetz, F., Nöthig, E.-M., Hellmann, S., Wiegmann, S., and Bracher, A.: Underway spectrophotometry in the Fram Strait (European Arctic Ocean): a highly resolved chlorophyll a data source for complementing satellite ocean color, Opt. Express, OE, 26, A678–A696, https://doi.org/10.1364/OE.26.00A678, 2018.

Macke, A. and Flores, H.: The Expeditions PS106/1 and 2 of the Research Vessel POLARSTERN to the Arctic Ocean in 2017, Bremerhaven, Germany, 171 pp., https://doi.org/10.2312/BzPM_0719_2018, 2018.

Malfatti, F., Lee, C., Tinta, T., Pendergraft, M. A., Celussi, M., Zhou, Y., Sultana, C. M., Rotter, A., Axson, J. L., Collins, D. B., Santander, M. V., Anides Morales, A. L., Aluwihare, L. I., Riemer, N., Grassian, V. H., Azam, F., and Prather, K. A.: Detection of Active Microbial Enzymes in Nascent Sea Spray Aerosol: Implications for Atmospheric Chemistry and Climate, Environ. Sci. Technol. Lett., 6, 171–177, https://doi.org/10.1021/acs.estlett.8b00699, 2019.

Mari, X., Passow, U., Migon, C., Burd, A. B., and Legendre, L.: Transparent exopolymer particles: Effects on carbon cycling in the ocean, Progress in Oceanography, 151, 13–37, https://doi.org/10.1016/j.pocean.2016.11.002, 2017.

Marks, R., Kruczalak, K., Jankowska, K., and Michalska, M.: Bacteria and fungi in air over the Gulf of Gdańsk and Baltic sea, Journal of Aerosol Science, 32, 237–250, https://doi.org/10.1016/S0021-8502(00)00064-1, 2001.

Matsuoka, A., Bricaud, A., Benner, R., Para, J., Sempéré, R., Prieur, L., Bélanger, S., and Babin, M.: Tracing the transport of colored dissolved organic matter in water masses of the Southern Beaufort Sea: relationship with hydrographic characteristics, Biogeosciences, 9, 925–940, https://doi.org/10.5194/bg-9-925-2012, 2012.

Matsuoka, A., Hooker, S. B., Bricaud, A., Gentili, B., and Babin, M.: Estimating absorption coefficients of colored dissolved organic matter (CDOM) using a semi-analytical algorithm for southern Beaufort Sea waters: application to deriving concentrations of dissolved organic carbon from space, Biogeosciences, 10, 917–927, https://doi.org/10.5194/bg-10-917-2013, 2013.

Matulová, M., Husárová, S., Capek, P., Sancelme, M., and Delort, A.-M.: Biotransformation of Various Saccharides and Production of Exopolymeric Substances by Cloud-Borne Bacillus sp. 3B6, Environ. Sci. Technol., 48, 14238–14247, https://doi.org/10.1021/es501350s, 2014.

May, N. W., Quinn, P. K., McNamara, S. M., and Pratt, K. A.: Multiyear study of the dependence of sea salt aerosol on wind speed and sea ice conditions in the coastal Arctic: ARCTIC SEA SALT AEROSOL, J. Geophys. Res. Atmos., 121, 9208–9219, https://doi.org/10.1002/2016JD025273, 2016.

Mayol, E., Arrieta, J. M., Jiménez, M. A., Martínez-Asensio, A., Garcias-Bonet, N., Dachs, J., González-Gaya, B., Royer, S.-J., Benítez-Barrios, V. M., Fraile-Nuez, E., and Duarte, C. M.: Long-range transport of airborne microbes over the global tropical and subtropical ocean, Nature Communications, 8, 1–9, https://doi.org/10.1038/s41467-017-00110-9, 2017.

McCarthy, M., Hedges, J., and Benner, R.: Major biochemical composition of dissolved high molecular weight organic matter in seawater, Marine Chemistry, 55, 281–297, https://doi.org/10.1016/S0304-4203(96)00041-2, 1996.

McCluskey, C. S., Hill, T. C. J., Humphries, R. S., Rauker, A. M., Moreau, S., Strutton, P. G., Chambers, S. D., Williams, A. G., McRobert, I., Ward, J., Keywood, M. D., Harnwell, J., Ponsonby, W., Loh, Z. M., Krummel, P. B., Protat, A., Kreidenweis, S. M., and DeMott, P. J.: Observations of Ice Nucleating Particles Over Southern Ocean Waters, Geophysical Research Letters, 45, 11,989-11,997, https://doi.org/10.1029/2018GL079981, 2018.

Mimura, T. and Romano, J. C.: Muramic Acid measurements for bacterial investigations in marine environments by high-pressure liquid chromatography, Appl. Environ. Microbiol., 50, 229–237, https://doi.org/10.1128/AEM.50.2.229-237.1985, 1985.

Mühlenbruch, M., Grossart, H.-P., Eigemann, F., and Voss, M.: Mini-review: Phytoplankton-derived polysaccharides in the marine environment and their interactions with heterotrophic bacteria, Environmental Microbiology, 20, 2671–2685, https://doi.org/10.1111/1462-2920.14302, 2018.

Müller, K., Lehmann, S., Pinxteren, D. van, Gnauk, T., Niedermeier, N., Wiedensohler, A., and Herrmann, H.: Particle characterization at the Cape Verde atmospheric observatory during the 2007 RHaMBLe intensive, Atmospheric Chemistry and Physics, 10, 2709–2721, https://doi.org/10.5194/acp-10-2709-2010, 2010.

Norris, S. J., Brooks, I. M., de Leeuw, G., Sirevaag, A., Leck, C., Brooks, B. J., Birch, C. E., and Tjernström, M.: Measurements of bubble size spectra within leads in the Arctic summer pack ice, Ocean Science, 7, 129–139, https://doi.org/10.5194/os-7-129-2011, 2011.

Notz, D. and Worster, M. G.: Desalination processes of sea ice revisited, Journal of Geophysical Research: Oceans, 114, https://doi.org/10.1029/2008JC004885, 2009.

Obernosterer, I., Catala, P., Lami, R., Caparros, J., Ras, J., Bricaud, A., Christine, D., Van Wambeke, F., and Lebaron, P.: Biochemical characteristics and bacterial community structure of the sea surface microlayer in the South Pacific Ocean, Biogeosciences, 5, 693–705, 2008.

O'Dowd, C. D., Facchini, M. C., Cavalli, F., Ceburnis, D., Mircea, M., Decesari, S., Fuzzi, S., Yoon, Y. J., and Putaud, J.-P.: Biogenically driven organic contribution to marine aerosol, Nature, 431, 676–680, https://doi.org/10.1038/nature02959, 2004.

Orellana, M. V., Matrai, P. A., Leck, C., Rauschenberg, C. D., Lee, A. M., and Coz, E.: Marine microgels as a source of cloud condensation nuclei in the high Arctic, PNAS, 108, 13612–13617, https://doi.org/10.1073/pnas.1102457108, 2011.

Panagiotopoulos, C. and Sempéré, R.: Analytical methods for the determination of sugars in marine samples: A historical perspective and future directions, Limnology and Oceanography: Methods, 3, 419–454, https://doi.org/10.4319/lom.2005.3.419, 2005.

Papakonstantinou-Presvelou, I., Sourdeval, O., and Quaas, J.: Strong Ocean/Sea-Ice Contrasts Observed in Satellite-Derived Ice Crystal Number Concentrations in Arctic Ice Boundary-Layer Clouds, Geophysical Research Letters, 49, e2022GL098207, https://doi.org/10.1029/2022GL098207, 2022.

Passow, U.: Transparent exopolymer particles (TEP) in aquatic environments, Progress in Oceanography, 55, 287–333, https://doi.org/10.1016/S0079-6611(02)00138-6, 2002.

Penner, J. E., Andreae, M. O., Annegarn, H., Barrie, L., Feichter, J., Hegg, D., Jayaraman, A., Leaitch, R., Murphy, D., Nganga, J., and Pitari, G.: Aerosols, their Direct and Indirect Effects, Climate Change 2001: The Scientific Basis. Contribution of Working Group I to the Third Assessment Report of the Intergovernmental Panel on Climate Change, 289–348, 2001.

Phongphattarawat, S.: Variability in pigment composition and bio-optical characteristics of phytoplankton populations in the Atlantic basin, http://purl.org/dc/dcmitype/Text, University of Oxford, 2016.

van Pinxteren, M., Müller, C., Iinuma, Y., Stolle, C., and Herrmann, H.: Chemical Characterization of Dissolved Organic Compounds from Coastal Sea Surface Microlayers (Baltic Sea, Germany), Environmental Science & Technology, 46, 10455–10462, https://doi.org/10.1021/es204492b, 2012.

van Pinxteren, M., Barthel, S., Fomba, K. W., Müller, K., Von Tümpling, W., and Herrmann, H.: The influence of environmental drivers on the enrichment of organic carbon in the sea surface microlayer and in submicron aerosol particles – measurements from the Atlantic Ocean, Elem Sci Anth, 5, https://doi.org/10.1525/elementa.225, 2017.

van Pinxteren, M., Robinson, T.-B., Zeppenfeld, S., Gong, X., Bahlmann, E., Fomba, K. W., Triesch, N., Stratmann, F., Wurl, O., Engel, A., Wex, H., and Herrmann, H.: High number concentrations of transparent exopolymer particles in ambient aerosol particles and cloud water – a case study at the tropical Atlantic Ocean, Atmospheric Chemistry and Physics, 22, 5725–5742, https://doi.org/10.5194/acp-22-5725-2022, 2022.

van Pinxteren, M., Zeppenfeld, S., Fomba, K. W., Triesch, N., Frka, S., and Herrmann, H.: Amino acids, carbohydrates, and lipids in the tropical oligotrophic Atlantic Ocean: sea-to-air transfer and atmospheric in situ formation, Atmospheric Chemistry and Physics, 23, 6571–6590, https://doi.org/10.5194/acp-23-6571-2023, 2023.

Piontek, J., Lunau, M., Händel, N., Borchard, C., Wurst, M., and Engel, A.: Acidification increases microbial polysaccharide degradation in the ocean, Biogeosciences, 7, 1615–1624, https://doi.org/10.5194/bg-7-1615-2010, 2010.

Porter, G. C. E., Adams, M. P., Brooks, I. M., Ickes, L., Karlsson, L., Leck, C., Salter, M. E., Schmale, J., Siegel, K., Sikora, S. N. F., Tarn, M. D., Vüllers, J., Wernli, H., Zieger, P., Zinke, J., and Murray, B. J.: Highly Active Ice-Nucleating Particles at the Summer North Pole, Journal of Geophysical Research: Atmospheres, 127, e2021JD036059, https://doi.org/10.1029/2021JD036059, 2022.

Prather, K. A., Bertram, T. H., Grassian, V. H., Deane, G. B., Stokes, M. D., DeMott, P. J., Aluwihare, L. I., Palenik, B. P., Azam, F., Seinfeld, J. H., Moffet, R. C., Molina, M. J., Cappa, C. D., Geiger, F. M., Roberts, G. C., Russell, L. M., Ault, A. P., Baltrusaitis, J., Collins, D. B., Corrigan, C. E., Cuadra-Rodriguez, L. A., Ebben, C. J., Forestieri, S. D., Guasco, T. L., Hersey, S. P., Kim, M. J., Lambert, W. F., Modini, R. L., Mui, W., Pedler, B. E., Ruppel, M. J., Ryder, O. S., Schoepp, N. G., Sullivan, R. C., and Zhao, D.: Bringing the ocean into the laboratory to probe the chemical complexity of sea spray aerosol, PNAS, 110, 7550–7555, https://doi.org/10.1073/pnas.1300262110, 2013.

Qin, G., Zhu, L., Chen, X., Wang, P. G., and Zhang, Y.: Structural characterization and ecological roles of a novel exopolysaccharide from the deep-sea psychrotolerant bacterium Pseudoalteromonas sp. SM9913, Microbiology, 153, 1566–1572, https://doi.org/10.1099/mic.0.2006/003327-0, 2007.

Quinn, P. K., Collins, D. B., Grassian, V. H., Prather, K. A., and Bates, T. S.: Chemistry and Related Properties of Freshly Emitted Sea Spray Aerosol, Chemical Reviews, 115, 4383–4399, https://doi.org/10.1021/cr500713g, 2015.

Rastelli, E., Corinaldesi, C., Dell'Anno, A., Lo Martire, M., Greco, S., Cristina Facchini, M., Rinaldi, M., O'Dowd, C., Ceburnis, D., and Danovaro, R.: Transfer of labile organic matter and microbes from the ocean surface to the marine aerosol: an experimental approach, Scientific Reports, 7, 1–10, https://doi.org/10.1038/s41598-017-10563-z, 2017.

Rérolle, V., Ruiz-Pino, D., Rafizadeh, M., Loucaides, S., Papadimitriou, S., Mowlem, M., and Chen, J.: Measuring pH in the Arctic Ocean: Colorimetric method or SeaFET?, Methods in Oceanography, 17, 32–49, https://doi.org/10.1016/j.mio.2016.05.006, 2016.

Robinson, T.-B., Wurl, O., Bahlmann, E., Jürgens, K., and Stolle, C.: Rising bubbles enhance the gelatinous nature of the air–sea interface, Limnology and Oceanography, 64, 2358–2372, https://doi.org/10.1002/lno.11188, 2019.

Rolph, R. J., Feltham, D. L., and Schröder, D.: Changes of the Arctic marginal ice zone during the satellite era, The Cryosphere, 14, 1971–1984, https://doi.org/10.5194/tc-14-1971-2020, 2020.

Röttgers, R., McKee, D., and Utschig, C.: Temperature and salinity correction coefficients for light absorption by water in the visible to infrared spectral region, Opt. Express, OE, 22, 25093–25108, https://doi.org/10.1364/OE.22.025093, 2014.

Röttgers, R., Doxaran, D., and Dupouy, C.: Quantitative filter technique measurements of spectral light absorption by aquatic particles using a portable integrating cavity absorption meter (QFT-ICAM), Opt. Express, OE, 24, A1–A20, https://doi.org/10.1364/OE.24.0000A1, 2016.

Russell, L. M., Hawkins, L. N., Frossard, A. A., Quinn, P. K., and Bates, T. S.: Carbohydrate-like composition of submicron atmospheric particles and their production from ocean bubble bursting, Proc. Natl. Acad. Sci. U.S.A., 107, 6652–6657, https://doi.org/10.1073/pnas.0908905107, 2010.

Šantl-Temkiv, T., Gosewinkel, U., Starnawski, P., Lever, M., and Finster, K.: Aeolian dispersal of bacteria in southwest Greenland: their sources, abundance, diversity and physiological states, FEMS Microbiol Ecol, 94, https://doi.org/10.1093/femsec/fiy031, 2018.

Šantl-Temkiv, T., Sikoparija, B., Maki, T., Carotenuto, F., Amato, P., Yao, M., Morris, C. E., Schnell, R., Jaenicke, R., Pöhlker, C., DeMott, P. J., Hill, T. C. J., and Huffman, J. A.: Bioaerosol field measurements: Challenges and perspectives in outdoor studies, Aerosol Science and Technology, 54, 520–546, https://doi.org/10.1080/02786826.2019.1676395, 2020.

Schiffer, J. M., Mael, L. E., Prather, K. A., Amaro, R. E., and Grassian, V. H.: Sea Spray Aerosol: Where Marine Biology Meets Atmospheric Chemistry, ACS Cent. Sci., 4, 1617–1623, https://doi.org/10.1021/acscentsci.8b00674, 2018.

Schill, S. R., Burrows, S. M., Hasenecz, E. S., Stone, E. A., and Bertram, T. H.: The Impact of Divalent Cations on the Enrichment of Soluble Saccharides in Primary Sea Spray Aerosol, Atmosphere, 9, 476, https://doi.org/10.3390/atmos9120476, 2018.

Schmale, J., Zieger, P., and Ekman, A. M. L.: Aerosols in current and future Arctic climate, Nature Climate Change, 11, 95–105, https://doi.org/10.1038/s41558-020-00969-5, 2021.

Schmithüsen, H.: Continuous meteorological surface measurement during POLARSTERN cruise PS106/1 (ARK-XXXI/1.1), https://doi.org/10.1594/PANGAEA.886302, 2018.

Schmithüsen, H.: Continuous meteorological surface measurement during POLARSTERN cruise PS106/2 (ARK-XXXI/1.2), https://doi.org/10.1594/PANGAEA.901179, 2019.

Schmitt-Kopplin, P., Liger-Belair, G., Koch, B. P., Flerus, R., Kattner, G., Harir, M., Kanawati, B., Lucio, M., Tziotis, D., Hertkorn, N., and Gebefügi, I.: Dissolved organic matter in sea spray: a transfer study from marine surface water to aerosols, Biogeosciences, 9, 1571–1582, 2012.

Sellegri, K., O'Dowd, C. D., Yoon, Y. J., Jennings, S. G., and Leeuw, G. de: Surfactants and submicron sea spray generation, Journal of Geophysical Research: Atmospheres, 111, https://doi.org/10.1029/2005JD006658, 2006.

Spencer, R. G. M., Aiken, G. R., Butler, K. D., Dornblaser, M. M., Striegl, R. G., and Hernes, P. J.: Utilizing chromophoric dissolved organic matter measurements to derive export and reactivity of dissolved organic carbon exported to the Arctic Ocean: A case study of the Yukon River, Alaska, Geophysical Research Letters, 36, https://doi.org/10.1029/2008GL036831, 2009.

Stedmon, C. A., Amon, R. M. W., Rinehart, A. J., and Walker, S. A.: The supply and characteristics of colored dissolved organic matter (CDOM) in the Arctic Ocean: Pan Arctic trends and differences, Marine Chemistry, 124, 108–118, https://doi.org/10.1016/j.marchem.2010.12.007, 2011.

Stein, A. F., Draxler, R. R., Rolph, G. D., Stunder, B. J. B., Cohen, M. D., and Ngan, F.: NOAA's HYSPLIT Atmospheric Transport and Dispersion Modeling System, Bull. Amer. Meteor. Soc., 96, 2059–2077, https://doi.org/10.1175/BAMS-D-14-00110.1, 2015.

Stolle, C., Nagel, K., Labrenz, M., and Jürgens, K.: Succession of the sea-surface microlayer in the coastal Baltic Sea under natural and experimentally induced low-wind conditions, Biogeosciences, 7, 2975–2988, https://doi.org/10.5194/bg-7-2975-2010, 2010.

Strong, C. and Rigor, I. G.: Arctic marginal ice zone trending wider in summer and narrower in winter, Geophysical Research Letters, 40, 4864–4868, https://doi.org/10.1002/grl.50928, 2013.

Sud, I. J. and Tyler, M. E.: Cell-Wall Composition and Osmotic Fragility of Selected Marine Bacteria, Journal of Bacteriology, 87, 696–700, 1964.

Suzuki, E. and Suzuki, R.: Variation of Storage Polysaccharides in Phototrophic Microorganisms, Journal of Applied Glycoscience, 60, 21–27, https://doi.org/10.5458/jag.jag.JAG-2012_016, 2013.

Taylor, B. B., Torrecilla, E., Bernhardt, A., Taylor, M. H., Peeken, I., Röttgers, R., Piera, J., and Bracher, A.: Bio-optical provinces in the eastern Atlantic Ocean and their biogeographical relevance, 8, 7165–7219, https://doi.org/10.5194/bgd-8-7165-2011, 2011.

Thomson, J.: Wave propagation in the marginal ice zone: connections and feedback mechanisms within the air–ice–ocean system, Philosophical Transactions of the Royal Society A: Mathematical, Physical and Engineering Sciences, 380, 20210251, https://doi.org/10.1098/rsta.2021.0251, 2022.

Triesch, N., van Pinxteren, M., Engel, A., and Herrmann, H.: Concerted measurements of free amino acids at the Cabo Verde islands: high enrichments in submicron sea spray aerosol particles and cloud droplets, Atmospheric Chemistry and Physics, 21, 163–181, https://doi.org/10.5194/acp-21-163-2021, 2021a.

Triesch, N., van Pinxteren, M., Frka, S., Stolle, C., Spranger, T., Hoffmann, E. H., Gong, X., Wex, H., Schulz-Bull, D., Gašparović, B., and Herrmann, H.: Concerted measurements of lipids in seawater and on submicrometer aerosol particles at the Cabo

Verde islands: biogenic sources, selective transfer and high enrichments, Atmospheric Chemistry and Physics, 21, 4267–4283, https://doi.org/10.5194/acp-21-4267-2021, 2021b.

Triesch, N., van Pinxteren, M., Salter, M., Stolle, C., Pereira, R., Zieger, P., and Herrmann, H.: Sea Spray Aerosol Chamber Study on Selective Transfer and Enrichment of Free and Combined Amino Acids, ACS Earth Space Chem., 5, 1564–1574, https://doi.org/10.1021/acsearthspacechem.1c00080, 2021c.

Trueblood, J. V., Wang, X., Or, V. W., Alves, M. R., Santander, M. V., Prather, K. A., and Grassian, V. H.: The Old and the New: Aging of Sea Spray Aerosol and Formation of Secondary Marine Aerosol through OH Oxidation Reactions, ACS Earth Space Chem., 3, 2307–2314, https://doi.org/10.1021/acsearthspacechem.9b00087, 2019.

Tynan, E., Clarke, J. S., Humphreys, M. P., Ribas-Ribas, M., Esposito, M., Rérolle, V. M. C., Schlosser, C., Thorpe, S. E., Tyrrell, T., and Achterberg, E. P.: Physical and biogeochemical controls on the variability in surface pH and calcium carbonate saturation states in the Atlantic sectors of the Arctic and Southern Oceans, Deep Sea Research Part II: Topical Studies in Oceanography, 127, 7–27, https://doi.org/10.1016/j.dsr2.2016.01.001, 2016.

Uetake, J., Hill, T. C. J., Moore, K. A., DeMott, P. J., Protat, A., and Kreidenweis, S. M.: Airborne bacteria confirm the pristine nature of the Southern Ocean boundary layer, PNAS, 117, 13275–13282, https://doi.org/10.1073/pnas.2000134117, 2020.

Vaqué, D., Boras, J. A., Arrieta, J. M., Agustí, S., Duarte, C. M., and Sala, M. M.: Enhanced Viral Activity in the Surface Microlayer of the Arctic and Antarctic Oceans, Microorganisms, 9, 317, https://doi.org/10.3390/microorganisms9020317, 2021.

Veron, F.: Ocean Spray, Annual Review of Fluid Mechanics, 47, 507–538, https://doi.org/10.1146/annurev-fluid-010814-014651, 2015.

Walker, S. A., Amon, R. M. W., and Stedmon, C. A.: Variations in high-latitude riverine fluorescent dissolved organic matter: A comparison of large Arctic rivers, Journal of Geophysical Research: Biogeosciences, 118, 1689–1702, https://doi.org/10.1002/2013JG002320, 2013.

Wang, X., Deane, G. B., Moore, K. A., Ryder, O. S., Stokes, M. D., Beall, C. M., Collins, D. B., Santander, M. V., Burrows, S. M., Sultana, C. M., and Prather, K. A.: The role of jet and film drops in controlling the mixing state of submicron sea spray aerosol particles, PNAS, 114, 6978–6983, https://doi.org/10.1073/pnas.1702420114, 2017.

Wendisch, M., Macke, A., Ehrlich, A., Lüpkes, C., Mech, M., Chechin, D., Dethloff, K., Barientos, C., Bozem, H., Brückner, M., Clemen, H.-C., Crewell, S., Donth, T., Dupuy, R., Ebell, K., Egerer, U., Engelmann, R., Engler, C., Eppers, O., Gehrmann, M., Gong, X., Gottschalk, M., Gourbeyre, C., Griesche, H., Hartmann, J., Hartmann, M., Heinold, B., Herber, A., Herrmann, H., Heygster, G., Hoor, P., Jafariserajehlou, S., Jäkel, E., Järvinen, E., Jourdan, O., Kästner, U., Kecorius, S., Knudsen, E. M., Köllner, F., Kretzschmar, J., Lelli, L., Leroy, D., Maturilli, M., Mei, L., Mertes, S., Mioche, G., Neuber, R., Nicolaus, M., Nomokonova, T., Notholt, J., Palm, M., van Pinxteren, M., Quaas, J., Richter, P., Ruiz-Donoso, E., Schäfer, M., Schmieder, K., Schnaiter, M., Schneider, J., Schwarzenböck, A., Seifert, P., Shupe, M. D., Siebert, H., Spreen, G., Stapf, J., Stratmann, F., Vogl, T., Welti, A., Wex, H., Wiedensohler, A., Zanatta, M., and Zeppenfeld, S.: The Arctic Cloud Puzzle: Using ACLOUD/PASCAL Multi-Platform Observations to Unravel the Role of Clouds and Aerosol Particles in Arctic Amplification, Bull. Amer. Meteor. Soc., https://doi.org/10.1175/BAMS-D-18-0072.1, 2018.

Wendisch, M., Brückner, M., Crewell, S., Ehrlich, A., Notholt, J., Lüpkes, C., Macke, A., Burrows, J. P., Rinke, A., Quaas, J., Maturilli, M., Schemann, V., Shupe, M. D., Akansu, E. F., Barrientos-Velasco, C., Bärfuss, K., Blechschmidt, A.-M., Block, K., Bougoudis, I., Bozem, H., Böckmann, C., Bracher, A., Bresson, H., Bretschneider, L., Buschmann, M., Chechin, D. G., Chylik, J., Dahlke, S., Deneke, H., Dethloff, K., Donth, T., Dorn, W., Dupuy, R., Ebell, K., Egerer, U., Engelmann, R., Eppers, O., Gerdes, R., Gierens, R., Gorodetskaya, I. V., Gottschalk, M., Griesche, H., Gryanik, V. M., Handorf, D., Harm-Altstädter, B., Hartmann, J., Hartmann, M., Heinold, B., Herber, A., Herrmann, H., Heygster, G., Höschel, I., Hofmann, Z., Hölemann, J., Hünerbein, A., Jafariserajehlou, S., Jäkel, E., Jacobi, C., Janout, M., Jansen, F., Jourdan, O., Jurányi, Z., Kalesse-Los, H., Kanzow, T., Käthner, R., Kliesch, L. L., Klingebiel, M., Knudsen, E. M., Kovács, T., Körtke, W., Krampe, D., Kretzschmar, J., Kreyling, D., Kulla, B., Kunkel, D., Lampert, A., Lauer, M., Lelli, L., Lerber, A. von, Linke, O., Löhnert, U., Lonardi, M., Losa, S. N., Losch, M., Maahn, M., Mech, M., Mei, L., Mertes, S., Metzner, E., Mewes, D., Michaelis, J., Mioche, G., Moser, M., Nakoudi, K., Neggers, R., Neuber, R., Nomokonova, T., Oelker, J., Papakonstantinou-Presvelou, I., et al.: Atmospheric and Surface Processes, and Feedback Mechanisms Determining Arctic Amplification: A Review of First Results and Prospects of the (AC)3 Project, Bulletin of the American Meteorological Society, 104, E208–E242, https://doi.org/10.1175/BAMS-D-21-0218.1, 2023.

Wietz, M., Wemheuer, B., Simon, H., Giebel, H.-A., Seibt, M. A., Daniel, R., Brinkhoff, T., and Simon, M.: Bacterial community dynamics during polysaccharide degradation at contrasting sites in the Southern and Atlantic Oceans, Environ. Microbiol., 17, 3822–3831, https://doi.org/10.1111/1462-2920.12842, 2015.

Wilbourn, E. K., Thornton, D. C. O., Ott, C., Graff, J., Quinn, P. K., Bates, T. S., Betha, R., Russell, L. M., Behrenfeld, M. J., and Brooks, S. D.: Ice Nucleation by Marine Aerosols Over the North Atlantic Ocean in Late Spring, Journal of Geophysical Research: Atmospheres, 125, e2019JD030913, https://doi.org/10.1029/2019JD030913, 2020.

Williams, P. M., Carlucci, A. F., Henrichs, S. M., Van Vleet, E. S., Horrigan, S. G., Reid, F. M. H., and Robertson, K. J.: Chemical and microbiological studies of sea-surface films in the Southern Gulf of California and off the West Coast of Baja California, Marine Chemistry, 19, 17–98, https://doi.org/10.1016/0304-4203(86)90033-2, 1986.

Wurl, O., Miller, L., Röttgers, R., and Vagle, S.: The distribution and fate of surface-active substances in the sea-surface microlayer and water column, Marine Chemistry, 115, 1–9, https://doi.org/10.1016/j.marchem.2009.04.007, 2009.

Wurl, O., Miller, L., and Vagle, S.: Production and fate of transparent exopolymer particles in the ocean, Journal of Geophysical Research: Oceans, 116, https://doi.org/10.1029/2011JC007342, 2011.

Xu, M., Tsona Tchinda, N., Li, J., and Du, L.: Insoluble lipid film mediates transfer of soluble saccharides from the sea to the atmosphere: the role of hydrogen bonding, Atmospheric Chemistry and Physics, 23, 2235–2249, https://doi.org/10.5194/acp-23-2235-2023, 2023.

Xu, W., Ovadnevaite, J., Fossum, K. N., Lin, C., Huang, R.-J., Ceburnis, D., and O'Dowd, C.: Sea spray as an obscured source for marine cloud nuclei, Nat. Geosci., 15, 282–286, https://doi.org/10.1038/s41561-022-00917-2, 2022.

Yang, X., Pyle, J. A., and Cox, R. A.: Sea salt aerosol production and bromine release: Role of snow on sea ice, Geophysical Research Letters, 35, https://doi.org/10.1029/2008GL034536, 2008.

Zábori, J., Matisāns, M., Krejci, R., Nilsson, E. D., and Ström, J.: Artificial primary marine aerosol production: a laboratory study with varying water temperature, salinity, and succinic acid concentration, Atmospheric Chemistry and Physics, 12, 10709–10724, https://doi.org/10.5194/acp-12-10709-2012, 2012.

Zäncker, B., Bracher, A., Röttgers, R., and Engel, A.: Variations of the Organic Matter Composition in the Sea Surface Microlayer: A Comparison between Open Ocean, Coastal, and Upwelling Sites Off the Peruvian Coast, Frontiers in Microbiology, 8, 2369, https://doi.org/10.3389/fmicb.2017.02369, 2017.

Zäncker, B., Cunliffe, M., and Engel, A.: Eukaryotic community composition in the sea surface microlayer across an east–west transect in the Mediterranean Sea, Biogeosciences, 18, 2107–2118, https://doi.org/10.5194/bg-18-2107-2021, 2021.

Zeppenfeld, S., van Pinxteren, M., Hartmann, M., Bracher, A., Stratmann, F., and Herrmann, H.: Glucose as a Potential Chemical Marker for Ice Nucleating Activity in Arctic Seawater and Melt Pond Samples, Environ. Sci. Technol., 53, 8747–8756, https://doi.org/10.1021/acs.est.9b01469, 2019a.

Zeppenfeld, S., van Pinxteren, M., Hartmann, M., Bracher, A., Wiegmann, S., Stratmann, F., and Herrmann, H.: Glucose, T50 and salinity in the surface microlayer and bulk water samples from the Arctic during POLARSTERN cruise PS106 (2017), https://doi.org/10.1594/PANGAEA.899258, 2019b.

Zeppenfeld, S., van Pinxteren, M., Engel, A., and Herrmann, H.: A protocol for quantifying mono- and polysaccharides in seawater and related saline matrices by electro-dialysis (ED) – combined with HPAEC-PAD, Ocean Science, 16, 817–830, https://doi.org/10.5194/os-16-817-2020, 2020.

Zeppenfeld, S., van Pinxteren, M., van Pinxteren, D., Wex, H., Berdalet, E., Vaqué, D., Dall'Osto, M., and Herrmann, H.: Aerosol Marine Primary Carbohydrates and Atmospheric Transformation in the Western Antarctic Peninsula, ACS Earth Space Chem., 5, 1032–1047, https://doi.org/10.1021/acsearthspacechem.0c00351, 2021a.

Zeppenfeld, S., Fuchs, S., Rödger, S., Dietze, A., van Pinxteren, M., and Herrmann, H.: Marine carbohydrates and inorganic ions in size-resolved atmospheric particles collected over the Southern Ocean, https://doi.org/10.1594/PANGAEA.927565, 2021b.

Zeppenfeld, S., van Pinxteren, M., Fuchs, S., Hartmann, M., Gong, X., and Herrmann, H.: Inorganic ions in fog water sampled from the Arctic in 2017, https://doi.org/10.1594/PANGAEA.932573, 2021c.

Zeppenfeld, S., van Pinxteren, M., Fuchs, S., Hartmann, M., Gong, X., and Herrmann, H.: Inorganic ions in size-resolved aerosol particles sampled from the Arctic in 2017, https://doi.org/10.1594/PANGAEA.932569, 2021d.

Zeppenfeld, S., van Pinxteren, M., Fuchs, S., Hartmann, M., and Herrmann, H.: Combined carbohydrates, dissolved free carbohydrates and pH in Arctic fog water sampled during PS106, https://doi.org/10.1594/PANGAEA.962208, 2023a.

Zeppenfeld, S., van Pinxteren, M., Fuchs, S., Hartmann, M., and Herrmann, H.: Combined carbohydrates, organic carbon and total aerosol mass concentrations in size-resolved aerosol particles sampled from the Arctic in 2017, https://doi.org/10.1594/PANGAEA.962210, 2023b.

Zeppenfeld, S., Bracher, A., Wiegmann, S., Zeising, M., Fuchs, S., van Pinxteren, M., and Herrmann, H.: Dissolved and particulate combined carbohydrates, pH, inorganic ions, CDOM and particulate absorption of SML and bulk water in Arctic surface seawater and melt ponds, https://doi.org/10.1594/PANGAEA.961004, 2023c.

Zinke, J., Salter, M. E., Leck, C., Lawler, M. J., Porter, G. C. E., Adams, M. P., Brooks, I. M., Murray, B. J., and Zieger, P.: The development of a miniaturised balloon-borne cloud water sampler and its first deployment in the high Arctic, Tellus B: Chemical and Physical Meteorology, 73, 1–12, https://doi.org/10.1080/16000889.2021.1915614, 2021.

Sebastian Zeppenfeld et al.

Correspondence to: Hartmut Herrmann (herrmann@tropos.de)

Figure SI 11. Cruise track during PS106 (blue), accompanied by with a closer zoomzoom-in view offor the ice floe camp from period (5 to –14 June 2017). Squares represent surface water sampling events (orange: ice-free ocean; red: open leads and polynyas within the pack ice; purple: melt ponds; green: MIZ) The red lines represent the ice edges on 07 June 2017 (west of Svalbard) and 07 July 2017 (east of Svalbard).

Formatiert: Schriftart: 9 Pt.

1591 Table SI 1. Detailed information about size-resolved aerosol particle sampling during PS106 campaign.

Start sampling[a]	Stop sampling[a]	Location	Residence time of air masses 12 h before sampling[b]				Wind speed (m s⁻¹)[e]	Air temperature (°C)[e]	Relative humidity (%)[e]	Percentage frequency of occurrence of fog[c,d] (%)	$Na^+_{aer,PM10}$ (ng m⁻³)[e]	$CCHO_{aer,PM10}$ (ng m⁻³)[e]	
			Ice-free (%)	MIZ (%)	Pack ice (%)	Land (%)							
24/05/17 20:49	26/05/17 16:34	North Sea	100	0	0	0	7.0±2.4	10.5±0.4	97±3	14.9	463	4.42	9.6E-03
26/05/17 19:34	29/05/17 11:33	Norwegian Sea	100	0	0	0	9.1±2.3	5.4±3.3	83±18	35.0	765	3.15	4.1E-03
29/05/17 12:46	01/06/17 08:28	Greenland Sea/ Fram Strait	50	9	29	13	9.9±3.8	-0.1±3.7	77±15	0.0	651	1.60	2.5E-03
01/06/17 09:35	04/06/17 08:06		3	20	76	0	7.2±3.0	-2.7±1.1	94±4	11.2	108	3.22	3.0E-02
04/06/17 10:57	07/06/17 08:08	Fram Strait/ Arctic Ocean (west and northwest of Svalbard)	0	1	99	0	5.2±2.1	-3.1±0.8	93±4	2.4	37	0.71	1.9E-02
07/06/17 09:39	10/06/17 08:29		0	1	99	0	4.5±1.6	-3.1±2.9	95±3	2.1	79	3.35	4.2E-02
10/06/17 09:25	13/06/17 11:23		0	0	100	0	6.2±3.0	-0.6±0.8	98±5	32.8	27	4.66	1.7E-01
13/06/17 12:36	16/06/17 08:18		0	0	100	0	4.3±1.5	-1.3±0.7	95±3	8.8	12	1.03	8.6E-02
16/06/17 09:13	19/06/17 09:03		2	42	56	0	4.0±1.3	-1.2±1.1	89±5	0.4	40	2.19	5.4E-02
19/06/17 10:00	25/06/17 09:30	Greenland Sea/Barents Sea	47	20	11	23	5.5±2.5	1.8±1.9	87±8	0.8	230	0.66	2.8E-03
25/06/17 11:40	28/06/17 09:20		11	35	54	0	6.2±2.5	-0.6±0.5	89±5	0.0	89	1.19	1.3E-02
28/06/17 10:20	04/07/17 08:55	Barents Sea/ Arctic Ocean (north and northeast of Svalbard)	2	5	93	1	6.0±1.7	-1.8±1.5	94±4	4.6	40	0.50	1.3E-02
04/07/17 10:25	07/07/17 08:45		0	0	100	0	5.9±1.3	-1.5±0.9	98±2	11.5	39	1.04	2.7E-02
07/07/17 09:50	13/07/17 09:00		0	9	87	4	6.9±2.1	-0.4±0.8	98±2	22.5	29	2.83	9.8E-02
13/07/17 10:05	16/07/17 10:35		10	42	40	8	7.7±3.5	0.5±1.1	95±6	8.0	269	3.14	1.2E-02

1592 [a] date/time format: dd/mm/yy hh:mm (UTC); [b] residence time of air masses over certain Earth surfaces were calculated based on back-trajectories and sea-ice maps using R; [c] meteorological data
1593 (mean ± standard deviation over sampling time) calculated from the quality controlled data archived in the PANGAEA network (Schmithüsen, 2018, 2019); [d] here, fog occurrence was defined based
1594 on two operational meteorological thresholds: visibility≤1500 m & relative humidity ≥98%; [e] values as the sum of all five Berner stages, size-resolved information are available on PANGAEA.

Table SI-2. Fog sampling during the PS106 campaign and average meteorological conditions at the sampling site calculated from the quality controlled data archived in the PANGAEA network (Schmithüsen, 2018, 2019); n.d.=not determined.

Start sampling[a]	Stop sampling[a]	Location	Time with fog events[b] (min)	Average wind speed during fog events (m s⁻¹)	Average air temperature during fog events (°C)	pH	$Na^+_{fog,liquid}$ (mg L⁻¹)	$Na^+_{fog,atmos}$ (ng m⁻³)	$CCHO_{fog,liquid}$ (µg L⁻¹)	$CCHO_{fog,atmos}$ (ng m⁻³)	$dFCHO_{fog,liquid}$ (µg L⁻¹)
26/05/17 04:33	26/05/17 12:27	North Sea	140	4.1	9.9	n.d.	91	61183	1976	1331.0	1539.4
26/05/17 18:48	27/05/17 12:26		1030	7.9	9.1	5.72	61	n.d	456	n.d	416.6
27/05/17 12:46	27/05/17 20:39	Norwegian Sea	240	8.2	9.1	5.74	23	22985	129	128.0	59.5
27/05/17 20:56	28/05/17 06:15		110	8.4	7.8	6.23	13	2823	153	32.9	104.9
01/06/17 13:15	02/06/17 16:37	Fram Strait/Arctic Ocean (west and northwest of Svalbard)	480	8.1	-1.1	6.41	903	150343	283	47.1	98.3
10/06/17 20:30	13/06/17 09:58		1410	3.9	-0.4	5.85	80	3723	186	8.7	104.3
23/06/17 10:00	25/06/17 10:10	Greenland Sea	30	4.4	-1.0	n.d.	448	72589	1542	250.1	233.5
25/06/17 10:30	29/06/17 10:34	Barents Sea/Arctic Ocean (north and northeast of Svalbard)	190	2.9	0.0	n.d.	393	n.d	726	n.d	93.9
29/06/17 10:45	01/07/17 10:25		190	5.6	-0.2	n.d.	374	73568	21818	4293.4	270.5
01/07/17 10:38	06/07/17 10:30		210	6.7	-1.5	n.d.	98	3902	467	18.7	40.4
06/07/17 10:45	07/07/17 11:10		280	5.6	-1.2	n.d.	90	7410	495	40.9	26.2
07/07/17 11:25	08/07/17 11:15		980	3.8	-0.4	6.44	30	377	322	4.1	488.0
08/07/17 11:30	08/07/17 22:20		240	6.8	-0.5	6.53	13	120	392	3.7	260.8
08/07/17 22:40	09/07/17 16:35		30	9.2	-2.9	n.d.	2.7	n.d.	363	n.d.	208.2
09/07/17 17:00	10/07/17 11:00		330	8.1	-0.6	6.75	5.1	185	81	3.0	84.1
10/07/17 11:15	11/07/17 11:00		250	9.0	0.0	6.26	19	1164	336	20.1	61.3

Formatiert: Block

11/07/17 11:15	14/07/17 10:25		200	7.3	-0.5	6.08	5.1	392	66	5.1	19.5
14/07/17 10:38	15/07/17 10:45		10	13.5	-0.1	6.12	7.6	2196	67	19.3	13.6
15/07/17 10:52	16/07/17 10:20	Barents Sea/Arctic Ocean (north and northeast of Svalbard	230	4.4	-0.2	6.14	18	3213	64	11.5	11.1
16/07/17 10:30	16/07/17 22:15		100	7.1	1.2	6.18	1.7	n.d	18	n.d	2.7
16/07/17 22:30	17/07/17 10:20		220	9.8	1.6	6.02	59	n.d	103	n.d	23.3
17/07/17 10:30	17/07/17 14:00		210	8.5	1.4	5.68	101	n.d	321	n.d	170.8

1597 [a] date/time format: dd/mm/yy hh:mm (UTC). [b] here, fog occurrence was defined based on two operational meteorological thresholds: visibility≤1500 m & relative humidity ≥98%.

1598

55

1599
1600
1601
1602
1603
1604
1605
1606
1607
1608
1609
1610
1611
1612
1613
1614
1615
1616
1617
1618
1619
1620
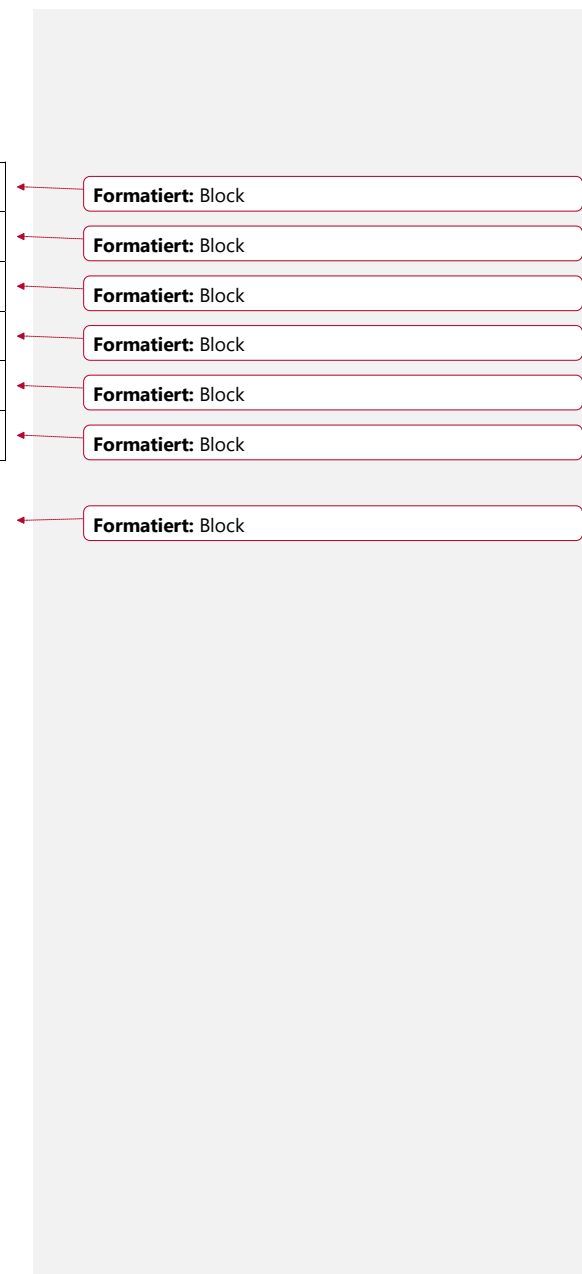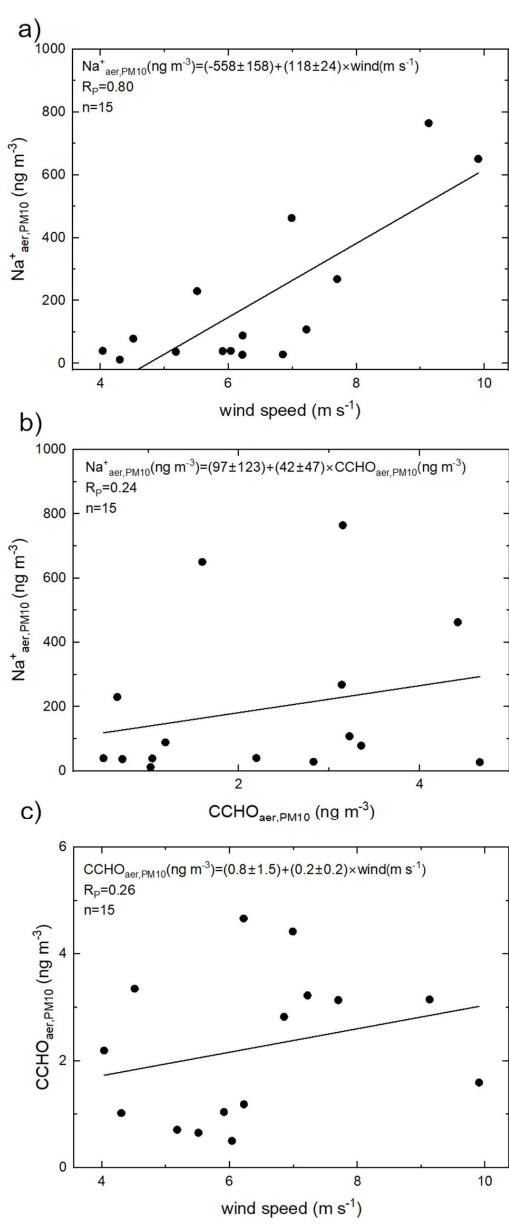
**Figure SI 32.** Correlations between a) $Na^+_{aer,PM10}$ and the averaged wind speed, b) $Na^+_{aer,PM10}$ and $CCHO_{aer,PM10}$, c) $CCHO_{aer,PM10}$ and averaged wind speed.
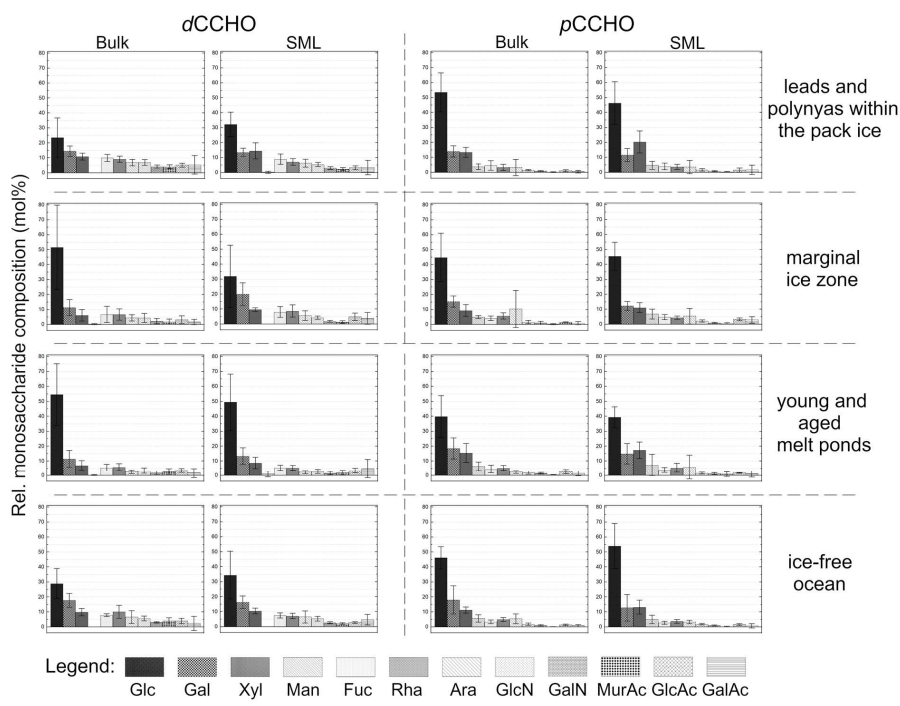
Figure SI 2. Relative monosaccharide composition of dissolved (*d*CCHO) and particulate combined carbohydrates (*p*CCHO) after acid hydrolysis in bulk and SML samples from the leads and polynyas within the pack ice, the MIZ, the ice-free ocean and young and aged melt ponds. The bar charts show the averages and standard deviations of the relative contributions.

Formatiert: Schriftart: Fett, Nicht Kursiv, Schriftfarbe: Text 1

Formatiert: Schriftfarbe: Text 1

Formatiert: Beschriftung
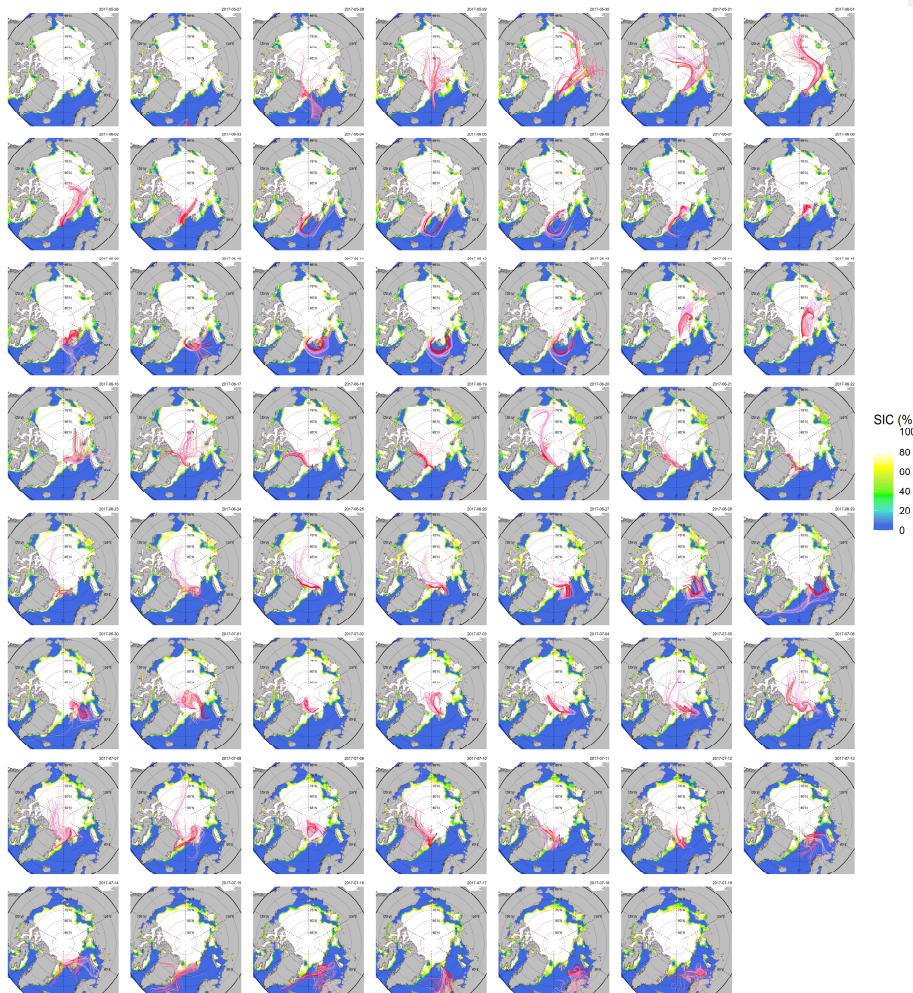
Figure SI 32. Daily sea ice maps for PS106 showing sea ice concentrations (SIC) and 120 h back-trajectories on an hourly basis at three arrival heights (red: 50 m, purple: 250 m and pink: 1000 m). A high-resolution animation can be viewed at the following link: https://doi.org/10.5446/62589

1626

1627

1628

1629

1630

1631

1632

1633

1634

1635

1636

1637

1638

1639

1640

1641

1642

1643

1644

1645

1646

1647

1648

1649

1650

1651

1652

a)

$a_{ph}440(\times10^{-3}\ m^{-1})=(16.2\pm3.0)+(0.22\pm0.02)\times p\text{CCHO}(\mu g\ L^{-1})$
$R_p=0.90$
$n=40$

$a_{ph}440\ (\times10^{-3}\ m^{-1})$

$p\text{CCHO}\ (\mu g\ L^{-1})$

b)

$a_{ph}440(\times10^{-3}\ m^{-1})=(13.1\pm3.9)+(0.12\pm0.01)\times \text{CCHO}(\mu g\ L^{-1})$
$R_p=0.84$
$n=40$

$a_{ph}440\ (\times10^{-3}\ m^{-1})$

$\text{CCHO}\ (\mu g\ L^{-1})$
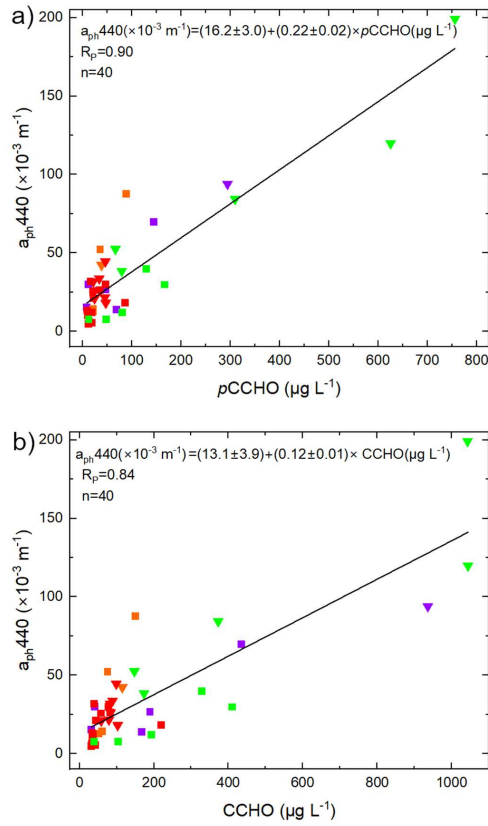
Figure SI 44. Correlation plots of $a_{ph}440$ derived from PAB spectra against a) pCCHO and b) CCHO. Triangles: SML, squares: bulk. Green: marginal ice zone (MIZ), purple: melt ponds, orange: ice-free ocean, red: open leads/polynyas in the pack ice.

1653

1654

1655

1656

1657

1658

1659

1660

a)

$a_{CDOM}350(\times10^{-3}\ m^{-1})=(100\pm19)+(1.0\pm0.1)\times d\text{CCHO}(\mu g\ L^{-1})$
$R_p=0.66$
$n=66$

$a_{CDOM}350\ (\times10^{-3}\ m^{-1})$

$d\text{CCHO}\ (\mu g\ L^{-1})$

b)

$a_{CDOM}443(\times10^{-3}\ m^{-1})=(15\pm2)+(0.07\pm0.01)\times d\text{CCHO}(\mu g\ L^{-1})$
$R_p=0.53$
$n=66$
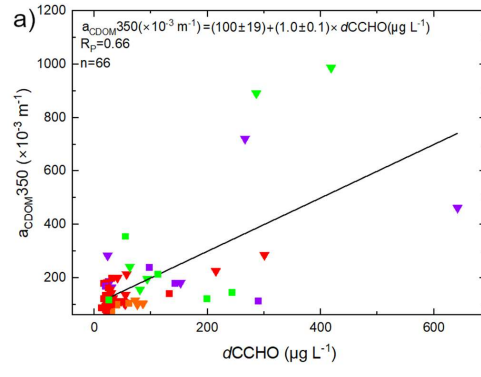
1661
1662
1663
1664
1665
1666
1667
1668
1669
1670
1671
1672
1673
1674
1675
1676

Figure SI 55. Correlation plots of a) $a_{CDOM}350$ against dCCHO, b) $a_{CDOM}443$ against dCCHO and c) $a_{CDOM}350$ against CCHO. Triangles: SML, squares: bulk. Green: marginal ice zone (MIZ), purple: melt ponds, orange: ice-free ocean, red: open leads/polynyas in the pack ice.
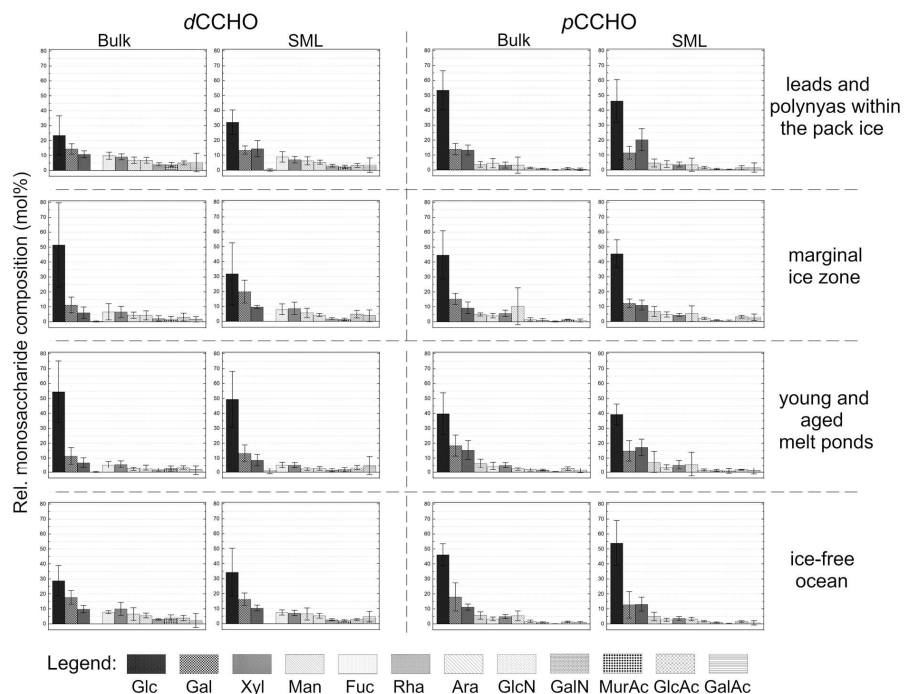
Figure SI 66. Relative monosaccharide composition of dissolved (*d*CCHO) and particulate combined carbohydrates (*p*CCHO) after acid hydrolysis in bulk and SML samples from the leads and polynyas within the pack ice, the MIZ, the ice-free ocean and young and aged melt ponds. The bar charts show the averages and standard deviations of the relative contributions.